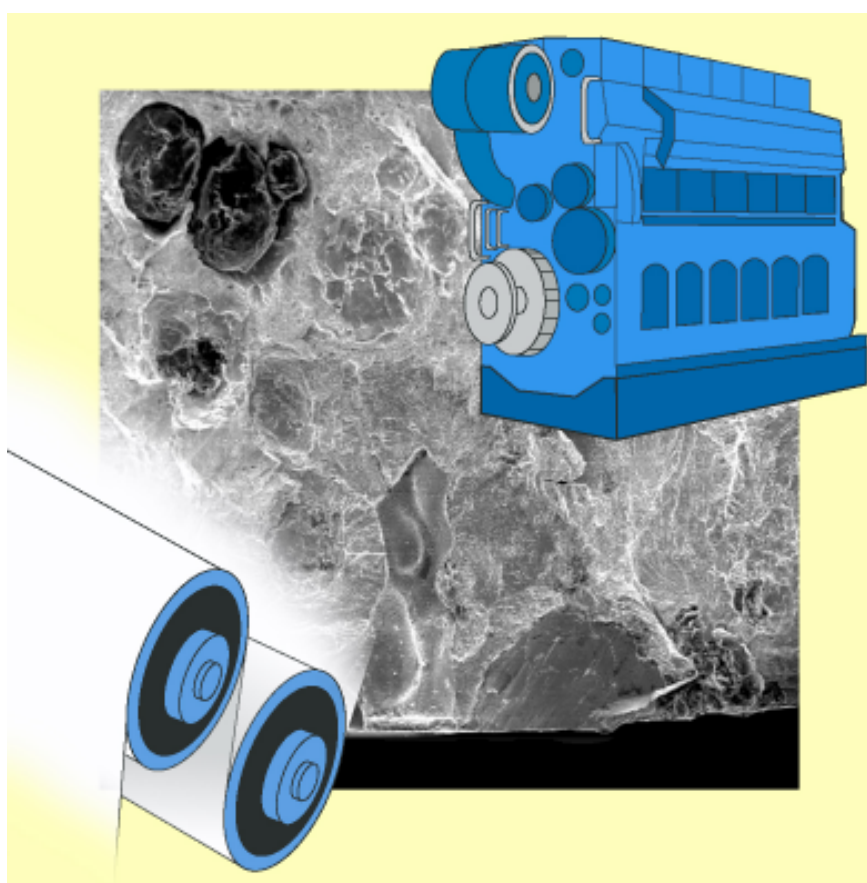Gary Marquis & Jussi Solin

# Long-life fatigue design of GRP 500 nodular cast iron components

# Long-life fatigue design of GRP 500 nodular cast iron components

Gary Marquis & Jussi Solin

VTT Manufacturing Technology

**VTT**

# Abstract

A project on Spheroidal Cast Iron in Long-Life Design was realised in 1997 to 1999. The goal was to gain understanding of the fatigue mechanisms and obtain high cycle design information on GRP500 nodular cast iron under both constant amplitude and variable amplitude loading. All the targets set at the beginning of the project have been achieved with the resources allocated. Several small but technically significant tasks have been added along the course of the project.

In total 332 fatigue tests, tension tests and extensive NDE studies on GRP 500 iron have been performed. The total number of fatigue cycles applied exceeded $3 \cdot 10^9$ cycles of which the majority were of variable amplitude such as may occur in rotating or reciprocating machines.

Empirical rules have been developed to predict the constant amplitude S-N curves for nodular iron in the range of $1 \cdot 10^4$ to $1 \cdot 10^6$ cycles to failure and for mean stresses in the range of 0 to 260 MPa. A new design tool for nodular cast irons has been proposed and verified for the two iron grades studied in this project. This design tool takes the form of the widely used Haigh diagram but takes into account material tensile strength, stress ratio, stress state (torsion or uniaxial) and specimen size effects.

Cycles as small as 60% of the constant amplitude fatigue limit were found to cause significant damage when as few as 1 of 300 000 cycles exceeds the fatigue limit. Miner's sums as low as 0.0001 produced fatigue failures. Similar measurements were made for both smooth and notched specimens.

# Preface

This report describes the experimental program and main results obtained within the research project SCILLED – Spheroidal Cast Iron in Long-Life Design. The work was performed mainly in VTT Manufacturing Technology during the period 1.9.1997 - 31.12.1999. Wärtsilä NSD, Valmet (currently Metso), VTT Automation and Helsinki University of Technology contributed in several sub-areas. The project has been funded by Tekes, Wärtsilä NSD, Valmet Rautpohja Foundry, Valmet Paper Machines and VTT Manufacturing Technology.

The intent of the project has been to develop useful data and approaches for the fatigue design of large castings produced from spheroidal graphite cast irons. Study has been limited to GRP 500. In particular, design rules related to the high cycle life regime were investigated. Fatigue data related to the combination of relatively large thermal induced mean stress changes and small high frequency stresses is not available in the open literature for this material and was of special interest. Several aspects of a successful fatigue design tool have been studied:

- effect of material grade and variations in microstructure,
- scatter in material strength and its influence on reliability of design,
- correlation between non-destructive testing results and fatigue endurance,
- effects of component size, notches and stress gradients, and
- influence of loading mode, occasional overloads or mean stress shifts.

As the project manager I'm grateful of the funding, co-operation and encouragement received in executing this both industrially and scientifically challenging project. The main contributors are named in the acknowledgements.

Espoo, fourth of July, 2000

Gary B. Marquis

# Contents

APPENDICES
Appendix A. NDT inspection report of casting with defects

# 1. Introduction

Nodular cast irons are used extensively in the production of paper machines and large diesel engines for power generation and marine propulsion. These two product groups were considered as target applications of this project. However, many of the results are directly applicable for other industries as well. Nodular iron is, for example, used in large gear boxes for windpower, which is a good example of applications with emphasised interest to weight reduction.

Casting provides an economical advantage over other production methods by offering significant freedom in geometrical shaping for functionality and for material utilisation. A good example is engine blocks, Fig.1. When compared to grey iron, nodular cast irons have significantly higher fatigue strengths, which provides great benefits in the design of rotating or reciprocating machinery. Different strength classes can be obtained by changing microstructure and properties of the iron matrix. From fatigue and ductility point of view, spheroidal graphite (SG) is much better than the graphite flakes of grey iron. This is a key element of nodular irons.

Diesel engines used in conjunction with electrical generators must often operate continuously for many tens of thousands of hours. High reliability of design is of primary interest, but the material strength shall be optimally utilised to obtain competitive products. Design optimisation for long lives requires an understanding of the high cycle fatigue behaviour of the cast material. Loading is primarily constant amplitude, but start-up and other transient events can result in occasional overloads which are known to greatly effect the fatigue performance of materials. Fatigue lives are typically computed even in billions of load cycles. Similar challenges are met in design of paper machines and gear boxes.

Rigid quality control during the casting process can eliminate the relatively large defects often associated with complex castings, but small microstructural irregularities can never be completely eliminated for large thick-section castings. These shrinkage pores, inclusions, and other types of naturally occurring defects have a controlling effect on the material endurance limit strength and its variation.

The current report describes the experimental program and the main results obtained within the research project SCILLED – Spheroidal Cast Iron in Long-Life Design. The intent of the project was to develop useful data and approaches for fatigue design of large castings produced of spheroidal graphite cast irons, in particular of GRP 500/ISO 1083.

A previous project and doctoral thesis (Marquis 1995) had shown that fatigue damage occurs well below the constant amplitude fatigue limit during variable amplitude loading of welds, both in structural and stainless steels. Some generally accepted assumptions behind the fatigue design rules had to be questioned there. The main target of the current SCILLED project was again to investigate the applicability of high cycle fatigue design rules, but now for spheroidal graphite cast iron. For this material, fatigue data related to the combination of relatively large thermal induced mean stress changes and small high frequency stresses was not available in the open literature, even though such data is of special interest to the target applications.

High reliability for a design can be obtained only by considering both mean material strength and normal scatter in material strength. For this reason significant attention was given to quantifying of scatter in material properties. An attempt was also made to clarify the possibilities for reducing the scatter through enhanced quality control of fatigue critical locations using modern non-destructive material testing technologies.

Several other aspects of a successful fatigue design tool have also been studied. One important aspect is Multiaxial loading (Socie & Marquis, 1999). Finally, a stage of knowledge was reached allowing a proposal of a "universal fatigue curve for GRP" as a revised form of the Haigh diagram. This and several other parts of the work are more fully developed in other reports and articles listed in the reference section of this report (Marquis, Rabb & Siivonen 1999, Marquis & Socie 1999). In the following, the experimental program and main results are described.
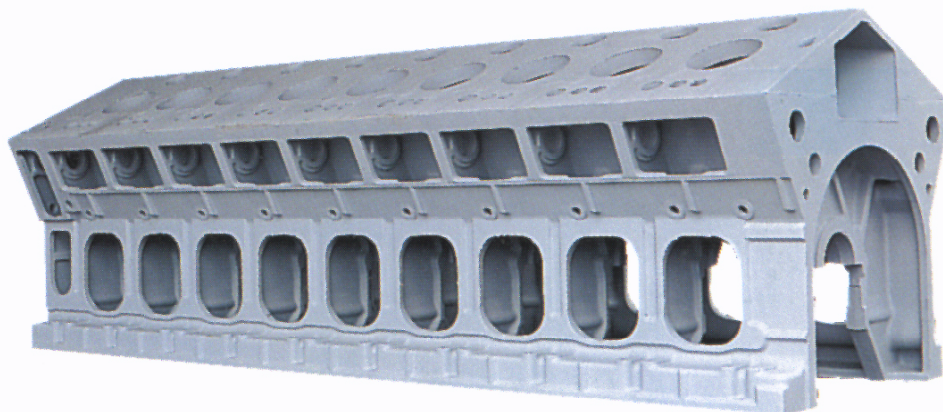


*Figure 1. Example of a heavy iron casting for fatigue loaded machinery. This diesel engine block is cast in the Valmet Rautpohja foundry for Wärtsilä NSD.*

# 2. Goals

The intent of this project has been to develop useful approaches for the fatigue design of large castings produced from spheroidal graphite, i.e., nodular cast irons. In particular, design rules related to the high cycle life regime will be investigated. The combination of relatively large thermal induced stress changes and small high frequency combustion or rotation induced stresses is of special interest. A successful fatigue design tool will be able to account for the following elements:

- material grade and variations in microstructure
- non-destructive testing results
- component size
- notches and stress gradients
- occasional overloads

The design value should be based both on expected mean life for the component and also on the expected scatter in fatigue strength. Material tests will be limited to nodular cast iron, GRP 500.

# 3. Experimental

In total 332 fatigue tests, 10 tension tests, detailed ultrasonic measurements on 36 specimens and extensive metallographic and fractographic studies of GRP 500 iron have been performed within this research project. The total number of fatigue cycles applied exceeded $3 \cdot 10^9$, of which the majority was variable amplitude such as may occur in rotating or reciprocating machines.

## 3.1 Test matrix

The original project plans approved by the steering group in early 1998 included fatigue tests on 245 specimens according to Tables 1 to 6. Several testing tasks were, however, expanded and others were added during the course of the project.

In Tables 1 to 6 the tests are specified by the geometries, characteristic dimensions and number of specimens together with target stress levels and cycle ratios. Some of the stress values have naturally been changed as appropriate during the project execution. All tests have been completed and reported in this report.

*Table 1. Supplement to Haigh diagram, smooth specimens.*

| n [1] | $K_t$ [2] | $\sigma_{mean}$ [3] | start $\sigma_a$ [4] | $\sigma_a$ increment |
|---|---|---|---|---|
| 15 | 1 | 260 | 126 | 8,5 |

*Table 2. Supplement to Haigh diagram, notched pieces.*

| n | $K_t$ | $\sigma_{mean}$ | start $\sigma_a$ | $\sigma_a$ increment |
|---|---|---|---|---|
| 15 | 1,705 | 260 | 75 | 8,5 |
| 15 | 1,705 | -200 | 250 | 22 |

---

[1] n is number of planned tests
[2] $K_t$ is the geometrical stress concentration factor of notch
[3] $\sigma_{mean}$ is mean stress;   all stress values given in MPa units
[4] $\sigma_a$ is stress amplitude, $(\sigma_{max} - \sigma_{min}) / 2$

*Table 3. Investigation of stress gradient and size effects, four point bend specimens.*

| n | b [5] | h | $\sigma_{mean}$ | $\sigma_a$ |
|---|---|---|---|---|
| 10 | 10 | 10 | 250 | 205 |
| 20 | 20 | 20 | 250 | 205 |
| 10 | 40 | 40 | 250 | 205 |

*Table 4. Investigation of long finite life regime.*

| n | $K_t$ | $\sigma_{mean}$ | $\sigma_{a,1}$ | $\sigma_{a,2}$ | $\sigma_{a,3}$ |
|---|---|---|---|---|---|
| 15 (5 at each level) | 1.0 | 182,5 | 137,5 | 172,5 | 227,5 |
| 15 (5 at each level) | 1.705 | 170 | 115 | 160 | 205 |
| 30 (10 at each level) | 1.0 | 260 | 110 | 130 | 240 |
| 30 (10 at each level) | 1.705 | 260 | 100 | 120 | 200 |

*Table 5. Variable amplitude testing with smooth specimen.*

| n | high cycle stresses | | low cycle stresses | | cycle ratio [6] |
|---|---|---|---|---|---|
| | $\sigma_{mean}$ | $\sigma_a$ | $\sigma_{mean}$ | $\sigma_a$ | $n_{hc}/n_{lc}$ |
| 10 | 260 | 111 | 190.5 | 180.5 | 3300 |
| 10 | 260 | 83.5 | 176,75 | 166,75 | 20000 |
| 10 | 260 | 65 | 167,5 | 157.5 | 300000 |

*Table 6. Variable amplitude testing with notched specimens.*

| n | high cycle stresses | | low cycle stresses | | cycle ratio |
|---|---|---|---|---|---|
| | $\sigma_{mean}$ | $\sigma_a$ | $\sigma_{mean}$ | $\sigma_a$ | $n_{hc}/n_{lc}$ |
| 10 | 260 | 95 | 182.5 | 172.5 | 3300 |
| 10 | 260 | 70 | 170 | 160 | 20000 |
| 10 | 260 | 55 | 162.5 | 152.5 | 300000 |

---

[5]  b and h indicate width and height of rectangular bend specimens
[6]  cycle ratio is given as $n_{hc}/n_{lc}$ , where $n_{hc}$ and $n_{lc}$ are number of high cycle and low cycle fatigue loads
     (HCF and LCF), respectively;   note that $\sigma_{a\,(HCF)} < \sigma_{a\,(LCF)}$

Tables 1 and 2 list the tests planned for refining the mean stress effects on fatigue strength of cast irons. The design criteria used in participating industry utilise the Haigh diagram to account for mean stress effect.

Table 3 lists the tests planned for determining the stress gradient and size effects by four point bending specimens.

The low cycle stress cycles included in the variable amplitude testing were reproduced under constant amplitude loading to find the basic S-N-curve. Table 4 gives the program for both the smooth and notched specimens.

The variable amplitude testing program is outlined in Tables 5 and 6. Definition of the terms describing the loading spectrum is given in Fig. 2.
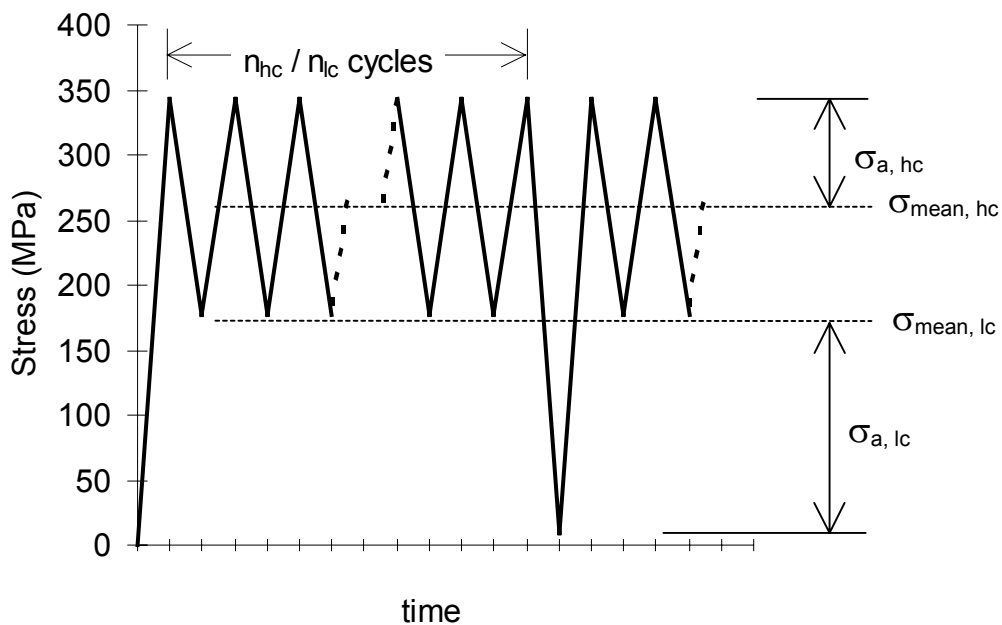


Figure 2. Definition of terms for the variable amplitude loading.

Static tensile testing was performed on 10 test bars taken from the $100 \times 100 \times 300$ ingots.

The originally planned NDT versus fatigue strength investigation was performed with the bend specimens (Table 3). In February 1999 it was decided to perform additional constant amplitude testing on 15 specimens with known large defects.

Finally, three small sets of tubular specimens were torsion fatigue tested to be able to assess the influence of stress state.

## 3.2  Test material and specimen numbering

The test material was spheroidal graphite cast iron GRP 500/ISO 1083. It was received in the form of ingots of three different sizes: 100×100×300 mm, 200×200×300 mm, and 50×200×300 mm. These dimensions are nominal. The ingots were provided by the Valmet Rautpohja Foundry. [7]

The specimen numbering system is intended to indicate ingot size (series), ingot number within the series and location from within the ingot where the specimen was taken. Specimen numbering is of the form *S.NN.LL* where *S* is the series number, *NN* is the ingot number within the series, and *LL* is the specimen location as indicated in Figs. 3 to 5. The series numbers are as follows:

S = 1:    100×100×300;

S = 2:    200×200×300, and

S = 3:    50×200×300.
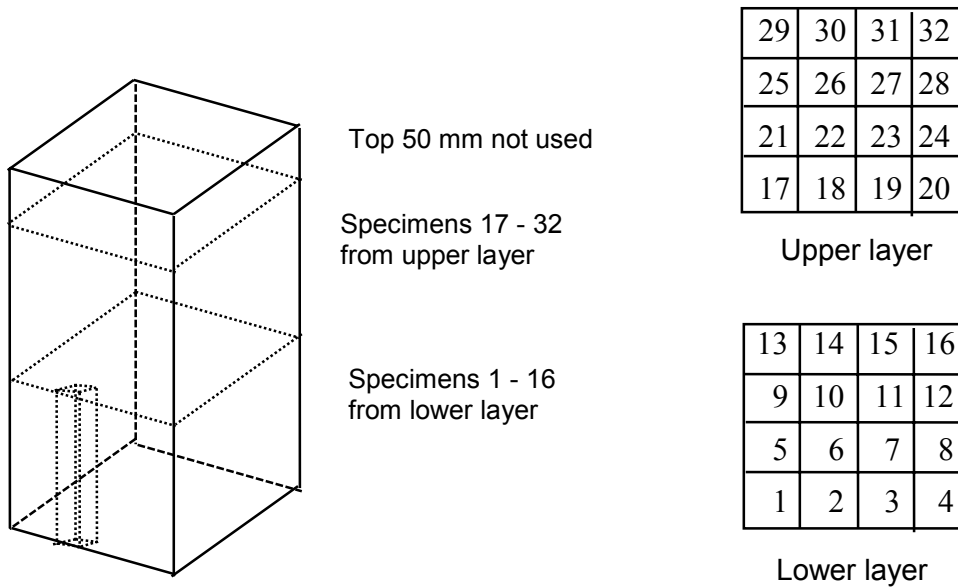


*Figure 3. Pattern for numbering round specimens taken from series 1 ingots.*

---

Specimens 80 - 99
from top 50 mm

| 93 | 94 | 95 | 96 |
|----|----|----|----|
| 83 | 84 | 85 | 86 |

| 57 | 58 | 59 | 60 | 61 | 62 | 63 | 64 |
|----|----|----|----|----|----|----|----|
| 49 | 50 | 51 | 52 | 53 | 54 | 55 | 56 |
| 41 | 42 | 43 | 44 | 45 | 46 | 47 | 48 |
| 33 | 34 | 35 | 36 | 37 | 38 | 39 | 40 |
| 25 | 26 | 27 | 28 | 29 | 30 | 31 | 32 |
| 17 | 18 | 19 | 20 | 21 | 22 | 23 | 24 |
| 9  | 10 | 11 | 12 | 13 | 14 | 15 | 16 |
| 1  | 2  | 3  | 4  | 5  | 6  | 7  | 8  |

Specimens 1 - 64
from lower layer
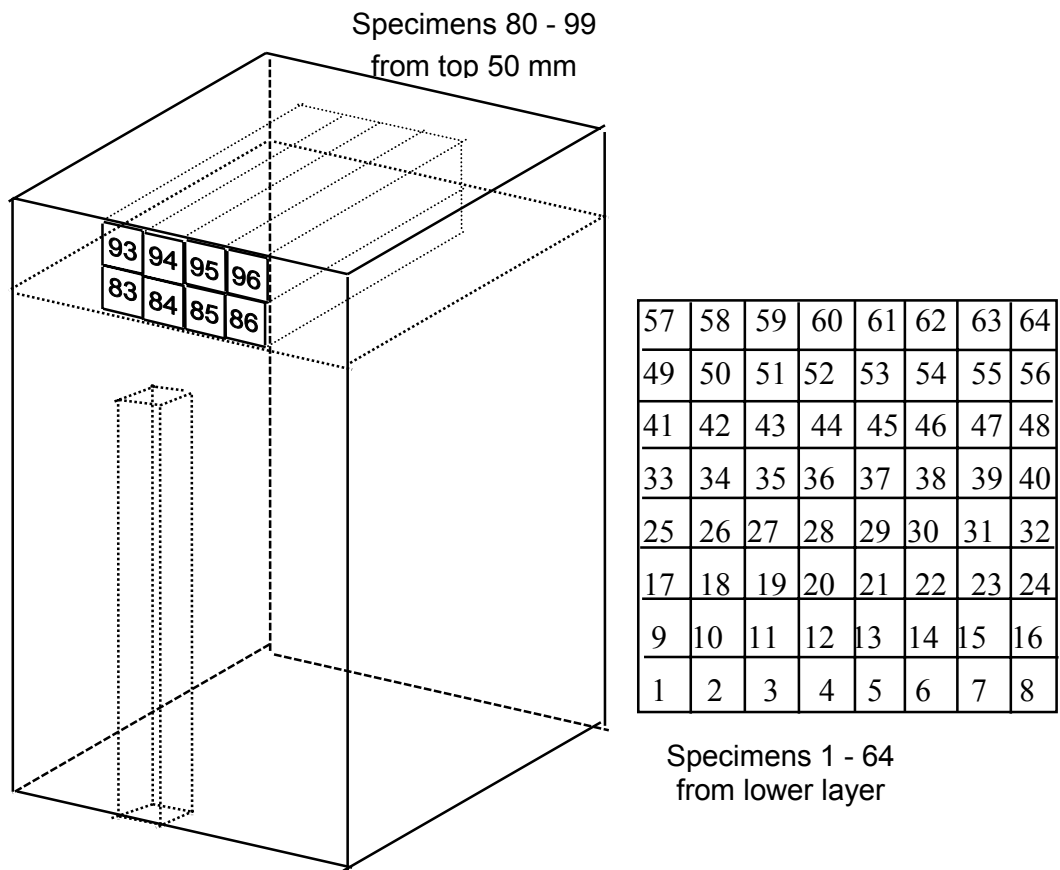
*Figure 4. Pattern for numbering bend specimens taken from series 2 ingots.*

Top 50 mm not used

| 01 | 02 | 03 | 04 | 05 | 06 | 07 | |
|----|----|----|----|----|----|----|--|
| 08 | 09 | 10 | 11 | 12 | 13 | 14 | |

Specimens 1 - 14
from lower layer
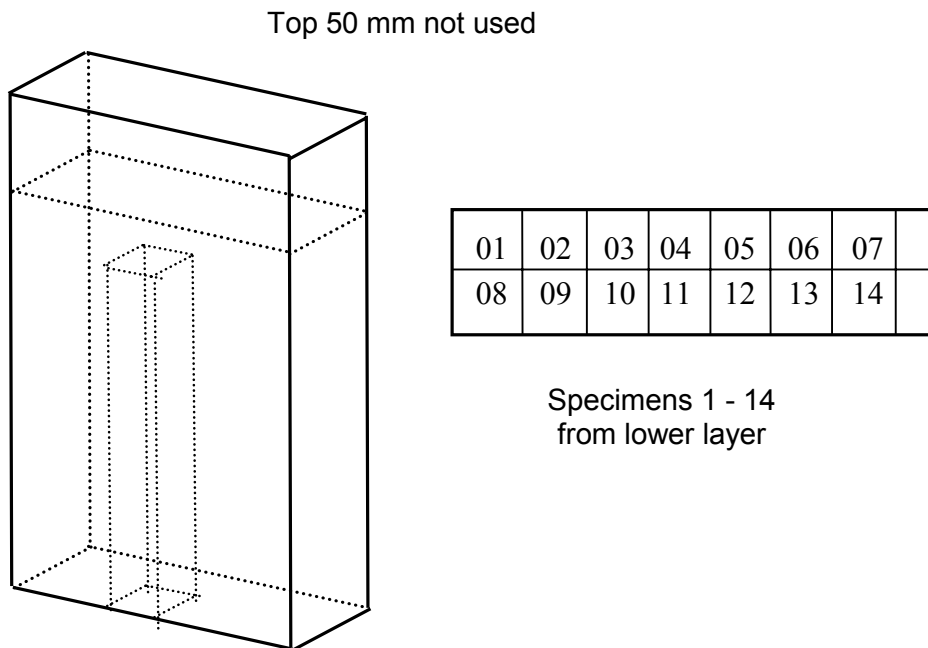
*Figure 5. Pattern for numbering bend specimens taken from series 3 ingots.*

## 3.3 Specimen geometries

Geometries for the fatigue specimens are shown in Figs. 6 to 8. Modified dimensions were used for part of the bending and torsion tests.
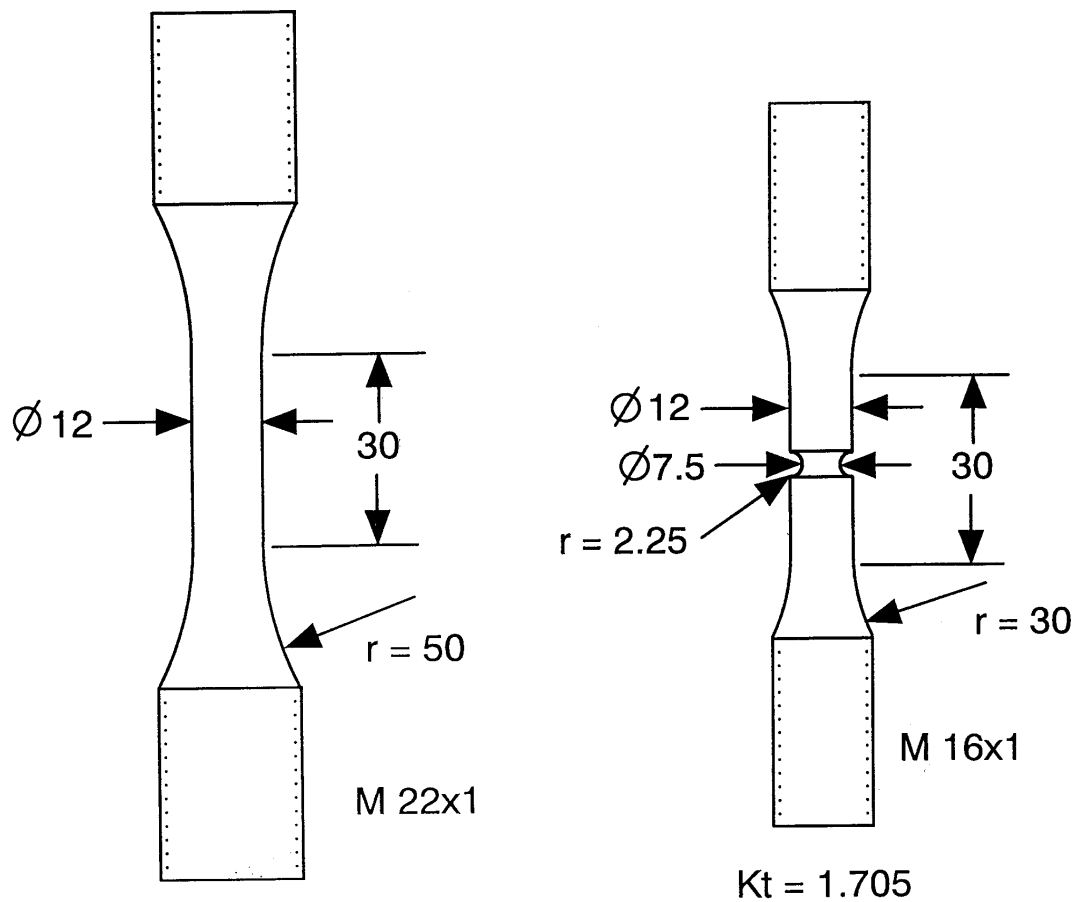


*Figure 6. a) smooth axial fatigue specimen; b) notched axial fatigue specimen.*
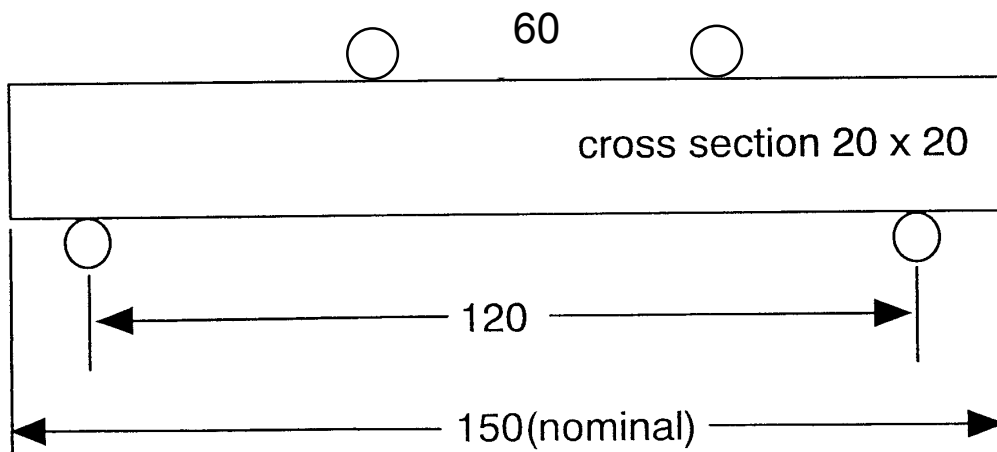
*Figure 7. Four-point bending rectangular cross section fatigue specimen.*
*Note that cross sections of 10×10 mm and 40×40mm were also used.*
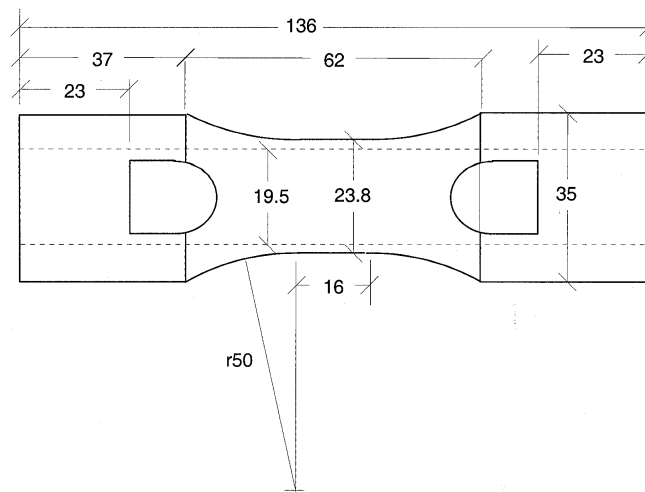


*Figure 8. Smooth tubular torsion fatigue specimen.*
*Note that gauge section diameter 25 mm was used for preliminary tests.*

## 3.4 Test machines and testing procedures

The vast majority of testing was performed using a programmable resonant test machine manufactured by RUMUL. This machine can perform constant amplitude testing at frequencies between 80 and 300 Hz. The axial specimens tested in this project were fatigued at a frequency of about 150 Hz.

Bend specimens and shear (torsion) tests were performed using an MTS series 810 digital servo-hydraulic test machine. These specimens were typically tested to fatigue lives of 2 million cycles or less which is easily done using servo-hydraulic machines. Tests longer than 2 million cycles are more appropriately done using the resonant machine due to its greater speed.

*Variable amplitude loading*

Because resonant testing was used also for the variable amplitude testing, short transients occur both before and after the application of each underload event. Underloads were achieved by quasi-statically altering the mean load on the specimen in the absence of resonance. Prior to the underload, the resonance excitation is removed causing a gradual decrease in cyclic amplitude within a few seconds. Similarly, after the underload, the resonant excitation is renewed and the amplitude gradually increases to the reported value.

Because of the high frequency, both reduced amplitude transients occupy 500 - 800 fatigue cycles. This, however, represents less than 1% of the total cycles in the load history. During the short transients the mean stress remained constant.

*Quality assurance*

The ability of the fatigue load frames to accurately reproduce the required load without unintended bending is of primary interest to be able to assess the significance of the results.

Fatigue test frames at VTT Manufacturing Technology are calibrated annually as required by VTT's quality manual. Load cells are required to have a maximum measurement error of 1% over measurement range. In practice it has been found that measurement error rarely exceeds 0.5%.

The load frames and specimen holders have been carefully aligned before testing. Furthermore, the loading principle of the resonant machine used for axial testing is flexible and unable to produce any significant bending moment. The servo-hydraulic test machine was used for bending and torsion testing. Due to the fixturing arrangements, also these tests are less sensitive to alignment.

# 4. Test results

## 4.1 Tensile tests

Static tensile testing was performed on ten test bars taken from the 100ˣ100ˣ300 ingots. The results are given Table 7.

*Table 7. Tensile test results.*

| Specimen | Dia. (mm) | $R_{p\,0.2}$ (MPa) | $R_{p\,1.0}$ (MPa) | $R_m$ (MPa) | strain (%) |
|---|---|---|---|---|---|
| 1.8.1 | 12.00 | 343 | 433 | 644 | 5.5 |
| 1.8.2 | 11.99 | 339 | 432 | 627 | 4.5 |
| 1.8.3 | 11.99 | 337 | 432 | 634 | - |
| 1.8.4 | 12.00 | 338 | 431 | 611 | 4.5 |
| 1.8.5 | 12.01 | 346 | 439 | 644 | 4.5 |
| 1.8.7 | 11.99 | 332 | 427 | 616 | 4.5 |
| 1.8.8 | 12.00 | 336 | 431 | 622 | 5 |
| 1.8.9 | 11.99 | 334 | 430 | 639 | 5.5 |
| 1.8.12 | 11.99 | 339 | 430 | 612 | 4.5 |
| 1.8.13 | 12.00 | 340 | 433 | 600 | 5.5 |
| **average** | **12.00** | **338** | **432** | **625** | |
| std. dev. | | 4.1 | 3.1 | 15 | |
| relative | | 1.2 % | 0.7 % | 2.4 % | |

The average ultimate tensile stress was 625 MPa with a standard deviation of 15 Mpa, which is 2.4 % of the mean. The scatters in the yield strength (0.2% plastic strain limit, $R_{p\,0.2}$) and flow stress at 1% plastic strain were clearly smaller. The average yield stress was 338 MPa with a unbiased standard deviation of 4.1 Mpa, i.e., 1.2 % of the mean.

## 4.2  Smooth specimens, constant amplitude

Constant amplitude fatigue life data for GRP 500 is given in Tables 8 to 12 and shown graphically in Fig. 9.

*Table 8. Constant amplitude fatigue test results with zero mean stress.*

| Specimen | $\sigma_{mean}$ | $\sigma_a$ | $N_f$ [8] | comments |
|----------|-----------------|------------|-----------|----------|
| 1.7.19 | 0 | 260 | 357 500 | |
| 1.7.20 | 0 | 242 | 1 513 700 | |
| 1.7.21 | 0 | 224.5 | 344 500 | |
| 1.7.22 | 0 | 207 | 49 500 | large defects |
| 1.7.23 | 0 | 207 | 928 700 | |
| 1.7.24 | 0 | 207 | 10 000 000 | no failure |
| 1.18.1 | 0 | 207 | 1 016 000 | |
| 1.4.16 | 0 | 290 | 283 000 | |
| 1.4.17 | 0 | 304 | 55 000 | |
| 1.4.18 | 0 | 294 | 5 000 | |
| 1.18.16 | 0 | 294 | 59 000 | |
| 1.18.20 | 0 | 294 | 118 000 | |
| 1.18.24 | 0 | 294 | 106 000 | |
| 1.18.28 | 0 | 294 | 132 000 | |
| 1.18.32 | 0 | 268 | 412 000 | |
| 1.4.01 | 0 | 259 | 502 000 | |
| 1.4.02 | 0 | 259 | 785 000 | |
| 1.4.03 | 0 | 259 | 375 000 | |
| 1.4.04 | 0 | 259 | 1 021 600 | |
| 1.4.05 | 0 | 259 | 982 000 | |
| 1.4.14 | 0 | 250 | 10 000 000 | no failure |

---

[8]  $N_f$  is the total number of cycles to failure

*Table 9. Long-life tests with pulsating tension load (R=0)[9].*

| Specimen | $\sigma_{mean}$ | $\sigma_a$ | $N_f$ | comments |
|----------|------|------|-------------|------------|
| 1.2.27 | 280 | 280 | 10 000 000 | no failure |
| 1.2.29 | 280 | 280 | 10 000 000 | no failure |
| 1.2.30 | 304 | 304 | 455 900 | |
| 1.2.31 | 280 | 280 | 695 500 | |
| 1.2.32 | 280 | 280 | 10 000 000 | no failure |
| 1.2.29* | 304 | 304 | 10 000 000 | no failure |
| 1.2.29* | 328 | 328 | 325 000 | |
| 1.2.32* | 304 | 304 | 4 683 000 | |

\* indicates re-testing of a previous non-failed specimen

*Table 10. Long-life tests with 182.5 MPa mean stress.*

| Specimen | $\sigma_{mean}$ | $\sigma_a$ | $N_f$ | comments |
|----------|------|-------|-------------|------------|
| 1.1.7 | 182,5 | 137,5 | 1 171 000 | |
| 1.1.8 | 182,5 | 137,5 | 982 000 | |
| 1.1.9 | 182,5 | 137,5 | 10 000 000 | no failure |
| 1.1.10 | 182,5 | 137,5 | 10 000 000 | no failure |
| 1.1.11 | 182,5 | 137,5 | 10 000 000 | no failure |
| 1.1.12 | 182,5 | 172,5 | 404000 | |
| 1.1.13 | 182,5 | 172,5 | 916000 | |
| 1.1.14 | 182,5 | 172,5 | 318000 | |
| 1.1.15 | 182,5 | 172,5 | 345000 | |
| 1.1.16 | 182,5 | 172,5 | 374000 | |
| 1.1.17 | 182,5 | 227,5 | 46000 | |
| 1.1.18 | 182,5 | 227,5 | 35000 | |
| 1.1.19 | 182,5 | 227,5 | 39000 | |
| 1.1.20 | 182,5 | 227,5 | 37000 | |
| 1.1.21 | 182,5 | 227,5 | 29000 | |

---

[9] R is the stress ratio: $\sigma_{min}$ / $\sigma_{max}$

*Table 11. Long-life tests with 260 MPa mean stress.*

| Specimen | $\sigma_{\mathbf{mean}}$ | $\sigma_{\mathbf{a}}$ | $N_f$ | comments |
|---|---|---|---|---|
| 1.2.6 | 260 | 130 | 518 000 | |
| 1.2.28 | 260 | 130 | 265 000 | |
| 1.3.5 | 260 | 130 | 448 000 | |
| 1.3.9 | 260 | 130 | 647 000 | |
| 1.3.20 | 260 | 130 | 431 000 | |
| 1.3.22 | 260 | 130 | 232 000 | |
| 1.3.25 | 260 | 130 | 277 000 | |
| 1.3.27 | 260 | 130 | 298 000 | |
| 1.3.28 | 260 | 130 | 378 000 | |
| 1.3.23 | 260 | 130 | 261 000 | |
| 1.4.8 | 260 | 130 | 437 400 | |
| 1.3.8 | 260 | 170 | 198 000 | |
| 1.3.11 | 260 | 170 | 168 000 | |
| 1.3.12 | 260 | 240 | 26 000 | |
| 1.3.13 | 260 | 240 | 13 300 | |
| 1.3.19 | 260 | 240 | 15 000 | |
| 1.3.24 | 260 | 240 | 12 200 | |
| 1.3.26 | 260 | 240 | 19 000 | |
| 1.3.29 | 260 | 240 | 10 300 | |
| 1.3.30 | 260 | 240 | 12 000 | |
| 1.3.31 | 260 | 240 | 19 400 | |
| 1.3.32 | 260 | 260 | 13 700 | |
| 1.2.18 | 260 | 110 | 845 000 | |
| 1.2.25 | 260 | 110 | 566 000 | |
| 1.3.7 | 260 | 110 | 2 630 000 | |
| 1.3.18 | 260 | 110 | 1 132 000 | |
| 1.2.3 | 260 | 110 | 1 501 000 | |
| 1.2.21 | 260 | 110 | 1 106 000 | |
| 1.3.10 | 260 | 110 | 10 000 000 | no failure |
| 1.3.15 | 260 | 110 | 532 000 | |
| 1.3.17 | 260 | 110 | 10 000 000 | no failure |
| 1.5.20 | 260 | 110 | 659 000 | |

*Table 12. Determination of $1 \cdot 10^7$ endurance limit at 260 MPa mean stress.*

| Specimen | $\sigma_{\text{mean}}$ | $\sigma_{\text{a}}$ | $N_f$ | comments |
|---|---|---|---|---|
| 1.1.6 | 260 | 125,5 | 589 000 | |
| 1.1.22 | 260 | 117 | 359 000 | |
| 1.1.23 | 260 | 108,5 | 1 332 000 | |
| 1.1.24 | 260 | 100 | 10 000 000 | no failure |
| 1.1.25 | 260 | 108,5 | 501 000 | |
| 1.1.26 | 260 | 100 | 11 000 000 | no failure |
| 1.1.27 | 260 | 108,5 | 705 000 | |
| 1.1.28 | 260 | 100 | 1 719 000 | |
| 1.1.29 | 260 | 91,5 | 10 000 000 | no failure |
| 1.1.30 | 260 | 100 | 12 000 000 | no failure |
| 1.1.31 | 260 | 108,5 | 1 106 000 | |
| 1.1.1* | 260 | 100 | 13 000 000 | no failure |
| 1.1.1* | 260 | 108,5 | 10 000 000 | no failure |
| 1.1.1* | 260 | 117 | 10 000 000 | no failure |
| 1.1.1* | 260 | 125,5 | 867 000 | |
| 1.1.2* | 260 | 108,5 | 10 000 000 | no failure |
| 1.1.2* | 260 | 117 | 2 457 000 | |

\* indicates re-testing of a previous non-failed specimen

## *Mean life S-N curves*

Based on the finite life data in Tables 8, 10 and 11, empirical rules can be derived to predict mean S-N curves for nodular iron in the range $1 \cdot 10^4 \leq N_f \leq 1 \cdot 10^6$ and for mean stresses in the range $0 \leq \sigma_{\text{mean}} \leq 260$ MPa. Assuming that the S-N curve takes the form

$$N_f = C\sigma_a^{\,b} \tag{1}$$

a fairly good correlation for all the data is found using the expression

$$N_f = 1000\left(\frac{\sigma_a}{\sigma_{fl}}\right)^b, \qquad \text{where} \tag{2}$$

$$b = \frac{-3}{\log\left[\dfrac{2\sigma_{fl}^2}{\Delta\sigma_w\left(\sigma_{fl}-\sigma_m\right)}\right]} \tag{3}$$
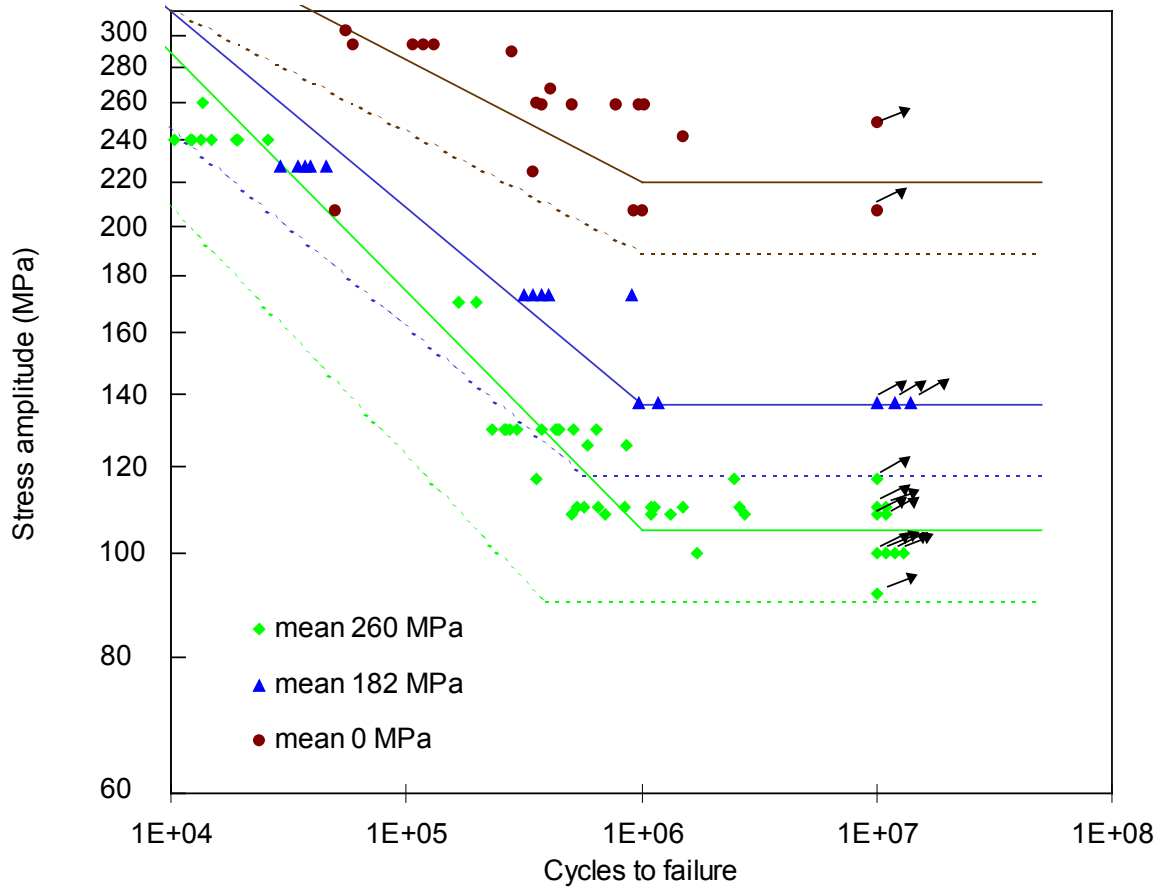
*Figure 9. Graphical presentation of constant amplitude smooth specimen data.*

In the case of the GRP 500, which was the test material in this study, it was found that $\Delta\sigma_w = 440$ MPa [10] and $\sigma_{fl} = 480$ MPa [11]. For the case of zero mean stress $b = -8.9$, for the case of $\sigma_m = 260$ MPa $b = -4.4$, and for the case of $\sigma_m = 180$ MPa $b = -5.5$.

Mean curves in the region $1 \cdot 10^4$ to $1 \cdot 10^6$ cycles to failure are shown in Fig. 9 as given by the equations

$$N_f = 7.3 x 10^{26} \sigma_a^{-8.9} \quad \text{for } \sigma_m = 0,$$

$$N_f = 5.6 x 10^{17} \sigma_a^{-5.5} \quad \text{for } \sigma_m = 182 \text{ MPa, and}$$

$$N_f = 6.3 x 10^{14} \sigma_a^{-4.4} \quad \text{for } \sigma_m = 260 \text{ MPa.}$$

---

[10] $\Delta\sigma_w$ is the stress range ($2^x$amplitude; $\sigma_{max} - \sigma_{min}$) at reversed loading endurance limit
[11] $\sigma_{fl}$ is the flow stress, i.e., average of the ultimate strength and yield strength

## Endurance limit

The endurance limits were determined by the staircase method using a test sequence shown in Fig. 10. For $\sigma_m$ = 260 MPa the $10^7$ cycles endurance limit stress is 107 MPa with a standard deviation of 11 MPa according to the staircase method. It shall be pointed out that reliable determination of the scatter in fatigue limit would be extremely expensive and that the given standard deviation is a rough estimate. Staircase method is, however, preferred for test series of this magnitude and it gives a relatively good estimate of the mean value (Rabb 1999 a,b,d).
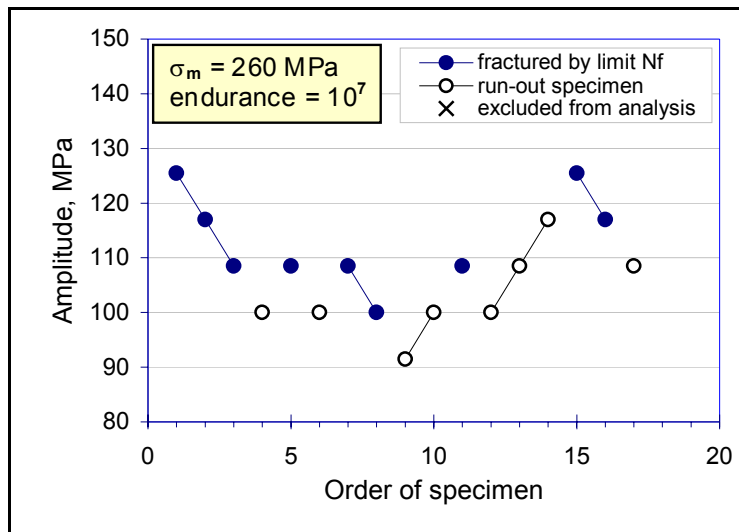


*Figure 10. Test sequence for endurance limit determination at 260 MPa mean stress.*

For other mean stresses endurance limit may be determined using the equation

$$\left( \frac{\Delta\sigma_a}{\Delta\sigma_w} + \frac{2 \cdot \sigma_m}{R_m + R_{p0.2}} \right) \cdot (1 - 0.25\lambda) = f \tag{4}$$

## Scatter in life

The solid lines in Fig. 9 are mean line curves, and cannot be used in design. Depending on the level of reliability required, design curves are normally reduced by two or three standard deviations (sd). The design values become then *mean - 2·sd* or *mean - 3·sd*.

If it is assumed that S-N data is log-normally distributed in life, and that scatter is independent of mean stress level in the region $0 \le \sigma_m \le 260$ MPa, a standard deviation in Log(C) can be obtained using linear regression as *sd*= 0,3.

The dashed lines in Fig. 9 are plotted as *mean - 2·sd*, where *sd* = 0,3 for the sloped portion of the curve, and assuming a 7% standard deviation in the endurance limit.

These lines appear to be slightly overconservative because the mean parameters from which the standard deviation was computed are based on Eq. 2.


## 4.3  Smooth specimens, variable amplitude

Variable amplitude testing has been performed on 41 smooth test specimens. Tests lasting longer than $150 \cdot 10^6$ fatigue cycles were stopped even if failure did not occur. The number of tests exceeds the planned number because of the difficulty in determining the stress and cycle ratio parameters. In principle, the cycle ratio, $n_{hc} / n_{lc}$, has been chosen to maintain a nearly constant number of overloads per test. This results in a relatively constant proportion of damage caused by the overload cycles. The large cycles contributed only a small portion of the calculated[12] fatigue damage, about 0.1% for the majority of the tests. Definition of the terms for describing the variable amplitude loading is given in Fig. 2. The results are given in Table 13.

*Table 13. Variable amplitude loading data of smooth specimens of GRP 500.*

| Specim. code | low cycle | | high cycle | | Endurance to failure | | | |
|---|---|---|---|---|---|---|---|---|
| | $\sigma_{mean, lc}$ MPa | $\sigma_{a, lc}$ MPa | $\sigma_{mean, hc}$ MPa | $\sigma_{a, hc}$ MPa | $\dfrac{n_{hc}}{n_{lc}}$ | $N_f$ cycles | $n_{lc}$ blocks | run-out? |
| 1.2.12 | 180.4 | 170.4 | 260 | 90,75 | 10 000 | 1 709 100 | 170 | |
| 1.2.8 | 180.4 | 170.4 | 260 | 90,75 | 10 000 | 5 998 000 | 599 | |
| 1.2.11 | 180.4 | 170.4 | 260 | 90,75 | 10 000 | 2 115 000 | 211 | |
| 1.2.14 | 180.4 | 170.4 | 260 | 90,75 | 100 000 | 47 800 000 | 478 | |
| 1.2.17 | 177.5 | 167 | 260 | 83,5 | 220 000 | 50 100 000 | 227 | |
| 1.2.24 | 177.5 | 167 | 260 | 83,5 | 220 000 | 17 139 000 | 77 | |
| 1.2.19 | 177.5 | 167 | 260 | 83,5 | 220 000 | 12 328 000 | 56 | |
| 1.2.23 | 177.5 | 167 | 260 | 83,5 | 220 000 | 3 906 700 | 17 | |
| 1.2.26 | 177.5 | 167 | 260 | 83,5 | 220 000 | 2 076 000 | 9 | |
| 1.2.2 | 177.5 | 167 | 260 | 83,5 | 220 000 | 76 606 000 | 348 | |
| 1.2.20 | 177.5 | 167 | 260 | 83,5 | 5 000 | 3 986 000 | 797 | |

(the table continues on next page)

---

[12] Damage sum $\Sigma(n_i / N_f) = 1$ at failure according to the linear cumulative damage model, i.e., Miner's rule.

*Table 13 continued. Variable amplitude loading data of smooth specimens.*

| Specim. code | low cycle | | high cycle | | Endurance to failure | | | |
|---|---|---|---|---|---|---|---|---|
| | $\sigma_{\text{mean, lc}}$ MPa | $\sigma_{\text{a, lc}}$ MPa | $\sigma_{\text{mean, hc}}$ MPa | $\sigma_{\text{a, hc}}$ MPa | $\dfrac{n_{\text{hc}}}{n_{\text{lc}}}$ | $N_{\text{f}}$ cycles | $n_{\text{lc}}$ blocks | run-out? |
| 1.2.15 | 177.5 | 167 | 260 | 83,5 | 20 000 | 5 717 000 | 285 | |
| 1.7.11 | 177.5 | 167 | 260 | 83,5 | 20 000 | 13 952 000 | 697 | |
| 1.7.12 | 177.5 | 167 | 260 | 83,5 | 20 000 | 4 594 100 | 229 | |
| 1.7.13 | 177.5 | 167 | 260 | 83,5 | 20 000 | 9 337 500 | 466 | |
| 1.7.14 | 177.5 | 167 | 260 | 83,5 | 20 000 | 4 332 900 | 216 | |
| 1.7.15 | 177.5 | 167 | 260 | 83,5 | 20 000 | 4 561 800 | 228 | |
| 1.7.16 | 177.5 | 167 | 260 | 83,5 | 20 000 | 5 308 800 | 265 | |
| 1.7.18 | 177.5 | 167 | 260 | 83,5 | 20 000 | 789 000 | 39 | |
| 1.7.17 | 177.5 | 167 | 260 | 83,5 | 20 000 | 3 493 000 | 174 | |
| 1.7.1 | 190 | 180.5 | 260 | 111 | 3300 | 462 400 | 140 | |
| 1.7.2 | 190 | 180.5 | 260 | 111 | 3300 | 300 000 | 90 | |
| 1.7.3 | 190 | 180.5 | 260 | 111 | 3300 | 625 000 | 189 | |
| 1.7.4 | 190 | 180.5 | 260 | 111 | 3300 | 950 000 | 287 | |
| 1.7.5 | 190 | 180.5 | 260 | 111 | 3300 | 653 000 | 197 | |
| 1.7.6 | 190 | 180.5 | 260 | 111 | 3300 | 602 000 | 182 | |
| 1.7.7 | 190 | 180.5 | 260 | 111 | 3300 | 385 000 | 116 | |
| 1.7.8 | 190 | 180.5 | 260 | 111 | 3300 | 582 000 | 176 | |
| 1.7.9 | 190 | 180.5 | 260 | 111 | 3300 | 520 200 | 157 | |
| 1.7.10 | 190 | 180.5 | 260 | 111 | 3300 | 600 000 | 181 | |
| 1.18.2 | 167.5 | 157.5 | 260 | 65 | 300 000 | 16 400 000 | 54 | |
| 1.18.4 | 167.5 | 157.5 | 260 | 65 | 300 000 | 48 500 000 | 161 | |
| 1.18.5 | 167.5 | 157.5 | 260 | 65 | 300 000 | 154 000 000 | 513 | **(R-O)** |
| 1.18.9 | 167.5 | 157.5 | 260 | 65 | 300 000 | 178 000 000 | 593 | **(R-O)** |
| 1.18.10 | 167.5 | 157.5 | 260 | 65 | 300 000 | 60 100 000 | 200 | |
| 1.18.13 | 167.5 | 157.5 | 260 | 65 | 300 000 | 184 000 000 | 613 | **(R-O)** |
| 1.18.14 | 167.5 | 157.5 | 260 | 65 | 300 000 | 186 000 000 | 620 | **(R-O)** |
| 1.18.15 | 167.5 | 157.5 | 260 | 65 | 300 000 | 110 000 000 | 366 | |
| 1.4.9 | 167.5 | 157.5 | 260 | 65 | 300 000 | 193 000 000 | 643 | **(R-O)** |
| 1.4.13 | 167.5 | 157.5 | 260 | 65 | 300 000 | 270 000 000 | 900 | **(R-O)** |

**(R-O)** indicates run-outs, i.e., without failure interrupted tests

Variable amplitude smooth specimen fatigue data is shown graphically in Fig. 11. Constant amplitude S-N lines from Fig. 9 are also shown in this figure. A few data points from Table 13 (specimens 1.2.8, 1.2.11 and 1.2.12) are not shown in this figure. These were the first tests using variable amplitude loading and the loading spectrum parameters were still being adjusted.
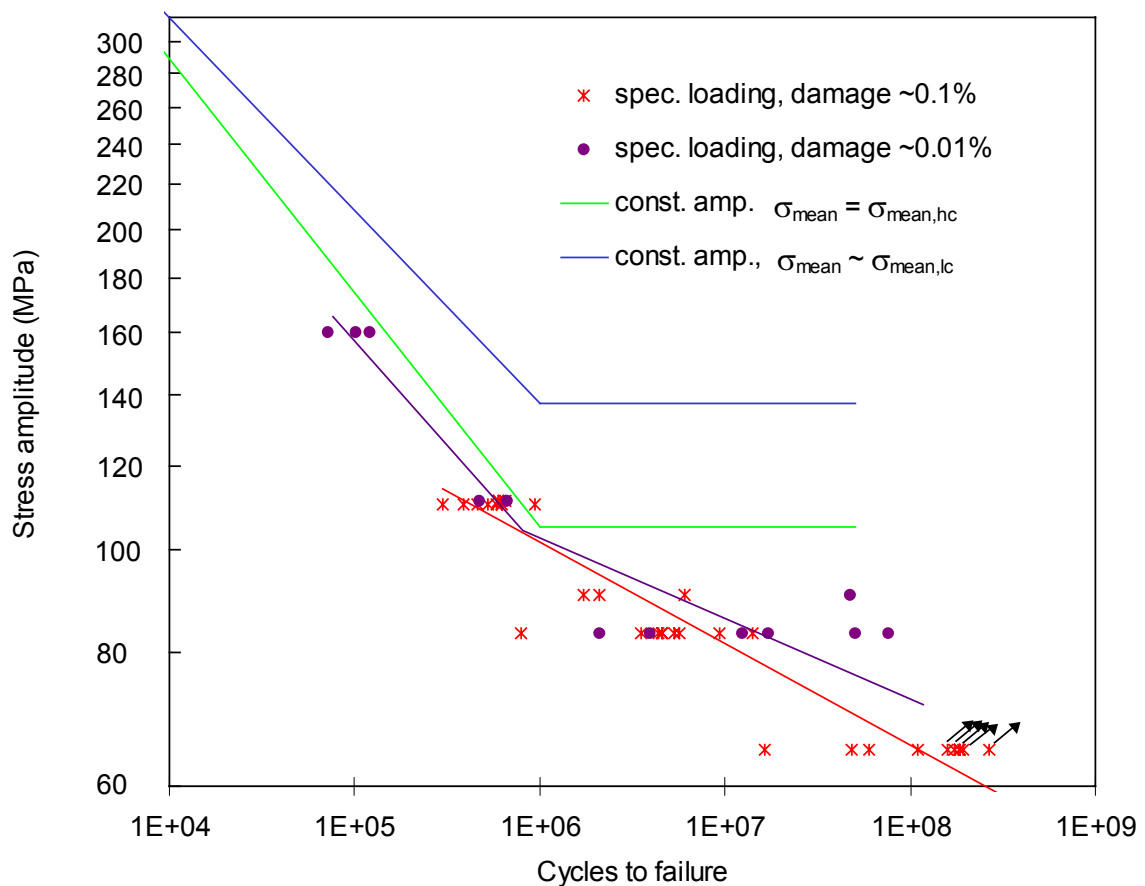


*Figure 11. Fatigue data for smooth specimens.*

## Mean life S-N curves

The mean curves presented in Fig. 11 were determined using the randomly censored maximum likelihood estimation (MML) technique as presented by Wallin (1999). This estimation technique has a benefit in that it is able to weigh also the contribution of run-outs to the statistical parameters. Fatigue life at a given stress value was assumed to be log-normally distributed. The equation can be presented as

$$\ln(L) = -n\ln\left(s\sqrt{2\pi}\right) - \sum_{i=1}^{n}\frac{\delta_i}{2}\left(\frac{\ln(\Delta\sigma_{eq,i}{}^b N_{f,i}) - m}{s}\right)^2 + \sum_{i=1}^{n}(1-\delta_i)\ln\left(\int_{\ln(\Delta\sigma_{eq,1}{}^b N_i)}^{\infty}\exp\left\{-\frac{1}{2}\left(\frac{x-m}{s}\right)^2\right\}dx\right)$$

(5)

where $\delta_i = 1$ for specimen resulting in failure and $\delta_i = 0$ for specimen with no failure, $\Delta\sigma_{eq,i}$ is the applied equivalent stress, $N_{f,i}$ is the life to failure and $N_i$ is number of cycles accumulated for a test that was stopped (censored). The terms $m$ and $s$ represent the mean and standard deviation of the logarithm of the random variable, $\Delta\sigma_{eq}{}^b N_f$. Values for $b$, $m$ and $s$ are determined iteratively such that the value of the estimator L obtains a maximum value.

In the event that all specimens result in failure, Eq. 5 reduces to a simple least squares fit, while if all specimens are run-outs it reduces to a deterministic model with the $m = \ln(\Delta\sigma_{eq}{}^b N_f)|^{max}$ for all specimens tested.

The lowest regression line in Fig. 11 is the best fit through the data points labelled 0.1% as determined using the maximum likelihood estimation (MML) technique and assuming an S-N relation

$$N_f = C\sigma_a{}^b \quad .$$

The resulting equation for the variable amplitude loading data is

$$N_f = 1.1x10^{27}\sigma_a{}^{-10.5} \quad .$$

*Scatter in life*

The standard deviation in $\mathrm{Log}(N_f)$ based on MML is 0.33 which is very close to a factor of two in life.

The data indicates that the scatter increases at lower stress levels. This obviously will have an effect of the eventual design line chosen and a MML method using non-constant scatter assumption can also be made. Rabb (1999b) has evaluated a portion of this data using a bi-linear S-N curve with one curve representing the data with fatigue lives exceeding $4.6\cdot10^6$ cycles to failure. This is also a valid interpretation of the data, especially in view of the 0.01% damage line which clearly shows a bilinear behaviour.

28

# 4.4  Notched specimens, constant amplitude

Tables 14 to 17 present the long life fatigue data for notched GRP500 specimens.

*Table 14. Long-life tests with notched specimens, 260 MPa mean stress.*

| Specimen | $\sigma_{mean}$ | $\sigma_a$ | $N_f$ | comments |
|----------|--------|--------|-----------|----------|
| 1.2.16 | 260 | 150 | 117 000 | |
| 1.4.10 | 260 | 150 | 145 000 | |
| 1.4.11 | 260 | 150 | 135 000 | |
| 1.4.12 | 260 | 170 | 69 000 | |
| 1.4.19 | 260 | 170 | 37 000 | |
| 1.4.20 | 260 | 170 | 54 000 | |
| 1.4.21 | 260 | 170 | 52 000 | |
| 1.4.22 | 260 | 170 | 62 000 | |
| 1.4.23 | 260 | 170 | 31 000 | |
| 1.4.24 | 260 | 170 | 48 000 | |
| 1.6.19 | 260 | 90 | 1 275 000 | |
| 1.6.20 | 260 | 90 | 695 000 | |
| 1.6.21 | 260 | 90 | 826 000 | |
| 1.6.22 | 260 | 90 | 835 000 | |
| 1.6.23 | 260 | 90 | 1 743 000 | |
| 1.6.24 | 260 | 90 | 1 356 000 | |
| 1.6.25 | 260 | 90 | 819 000 | |
| 1.6.26 | 260 | 90 | 1 056 000 | |
| 1.6.27 | 260 | 90 | 835 000 | |
| 1.6.28 | 260 | 90 | 1 457 000 | |
| 1.6.29 | 260 | 120 | 382 000 | |
| 1.6.30 | 260 | 120 | 245 000 | |
| 1.6.31 | 260 | 120 | 264 000 | |
| 1.6.32 | 260 | 120 | 200 000 | |
| 1.2.1 | 260 | 120 | 426 000 | |
| 1.2.4 | 260 | 120 | 519 000 | |
| 1.2.5 | 260 | 120 | 320 000 | |
| 1.2.9 | 260 | 120 | 265 000 | |
| 1.2.10 | 260 | 120 | 272 000 | |
| 1.2.13 | 260 | 120 | 485 000 | |

*Table 15. Long-life tests with notched specimens, 200 MPa mean stress.*

| Specimen | $\sigma_{mean}$ | $\sigma_a$ | $N_f$ | comments |
|----------|-----------------|------------|-------|----------|
| 1.6.16 | 200 | 272 | 7 400 | |
| 1.6.17 | 200 | 228 | 22 000 | |
| 1.6.18 | 200 | 184 | 58 000 | |

*Table 16. Long-life tests with notched specimens, 170 MPa mean stress.*

| Specimen | $\sigma_{mean}$ | $\sigma_a$ | $N_f$ | comments |
|----------|-----------------|------------|-------|----------|
| 1.11.5 | 170 | 230 | 19 000 | |
| 1.11.6 | 170 | 120 | 1 250 000 | run-out |
| 1.11.7 | 170 | 125 | 398 000 | |
| 1.11.8 | 170 | 125 | 372 000 | |
| 1.11.9 | 170 | 125 | 335 000 | |
| 1.11.10 | 170 | 120 | 537 000 | |
| 1.11.11 | 170 | 120 | 399 000 | |
| 1.11.16 | 170 | 120 | 1 178 000 | |
| 1.3.1 | 170 | 160 | 126 000 | |
| 1.3.2 | 170 | 160 | 326 000 | |
| 1.3.3 | 170 | 170 | 135 000 | |
| 1.3.4 | 170 | 170 | 93 000 | |
| 1.3.6 | 170 | 170 | 93 000 | |
| 1.3.14 | 170 | 230 | 31 000 | |
| 1.3.16 | 170 | 230 | 42 000 | |
| 1.3.21 | 170 | 230 | 24 000 | |
| 1.5.3 | 170 | 230 | 36 000 | |

*Table 17. Endurance limit testing with notched specimens for mean stresses –200 MPa and 260 MPa.*

| Specimen | $\sigma_{mean}$ | $\sigma_a$ | $N_f$ | comments |
|---|---|---|---|---|
| 1.4.25 | -200 | 250 | 1 038 000 | |
| 1.4.26 | -200 | 228 | 18 500 000 | run-out |
| 1.4.27 | -200 | 250 | 352 000 | |
| 1.4.28 | -200 | 228 | 12 126 000 | failure! |
| 1.4.29 | -200 | 250 | 1 386 000 | |
| 1.4.30 | -200 | 228 | 3 474 000 | |
| 1.4.31 | -200 | 206 | 20 000 000 | run-out |
| 1.4.32 | -200 | 228 | 24 000 000 | run-out |
| 1.5.34 | -200 | 250 | 636 000 | |
| 1.5.33 | -200 | 228 | 10 000 000 | run-out |
| 1.5.30 | -200 | 250 | 786 000 | |
| 1.5.29 | -200 | 228 | 138 000 | |
| 1.5.15 | -200 | 206 | 10 000 000 | run-out |
| 1.5.12 | -200 | 228 | 7 131 000 | |
| 1.5.10 | -200 | 206 | 24 000 000 | run-out |
| 1.6.1 | 260 | 83,5 | 10 000 000 | no failure |
| 1.6.2 | 260 | 100,5 | 431 000 | |
| 1.6.3 | 260 | 92 | 2 101 000 | |
| 1.6.4 | 260 | 83,5 | 2 044 000 | |
| 1.6.5 | 260 | 75 | 10 000 000 | no failure |
| 1.6.6 | 260 | 83,5 | 2 288 000 | |
| 1.6.7 | 260 | 75 | 11 000 000 | no failure |
| 1.6.8 | 260 | 83,5 | 3 076 000 | |
| 1.6.9 | 260 | 75 | 12 000 000 | no failure |
| 1.6.10 | 260 | 83,5 | 1 612 000 | |
| 1.6.11 | 260 | 75 | 13 000 000 | no failure |
| 1.6.12 | 260 | 83,5 | 11 000 000 | no failure |
| 1.6.13 | 260 | 92 | 1 650 000 | |
| 1.6.14 | 260 | 83,5 | 9 204 000 | |
| 1.6.15 | 260 | 75 | 14 000 000 | no failure |

*Mean life S-N curves*

The data given in Tables 14 to 17 for determining long life fatigue curves and endurance limit of notched GRP500 specimens is shown graphically in Fig. 12.
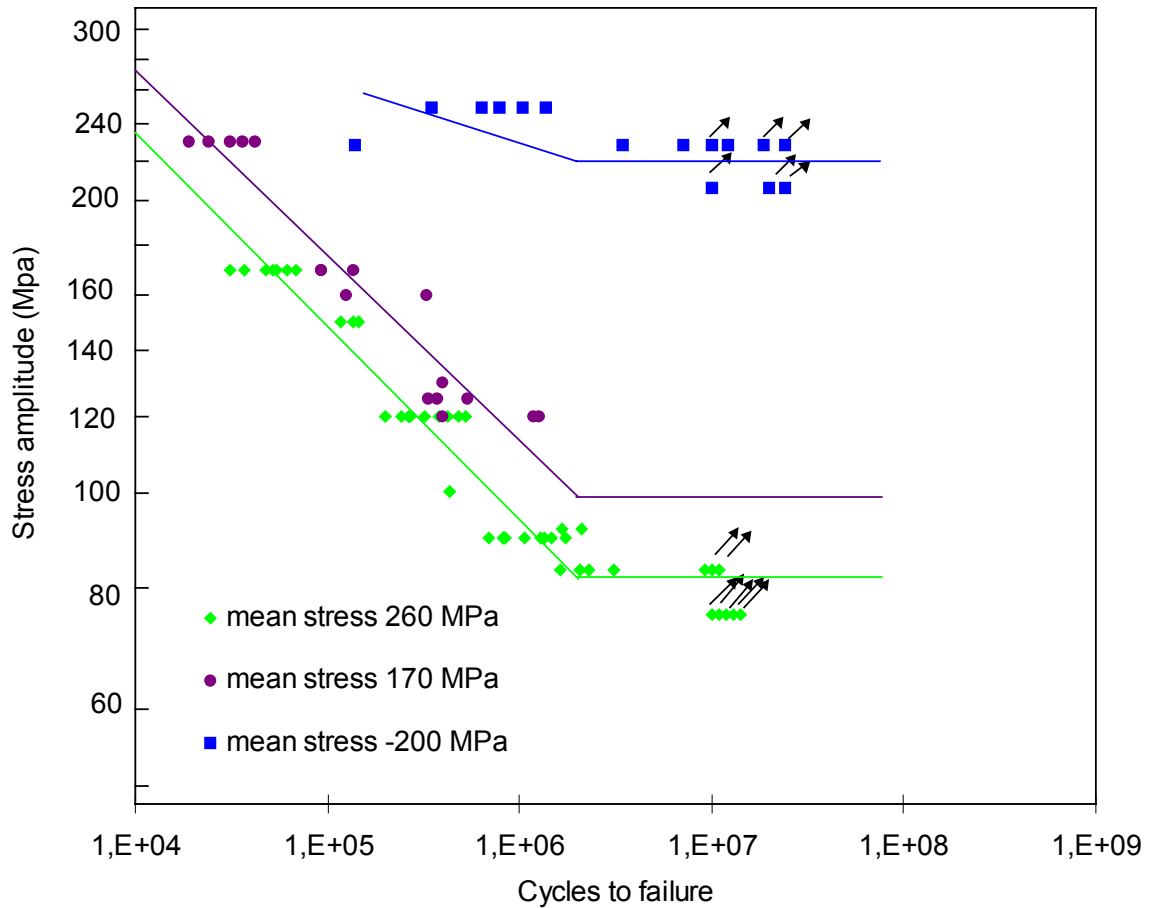


*Figure 12. Constant amplitude data of notched GRP 500 specimens.*

S-N curves in the region $1 \cdot 10^{4}$ to $2 \cdot 10^{6}$ cycles to failure shown in Fig. 12 are given by the equations

$$N_f = 5.8 x 10^{16} \sigma_a^{-5.2} \quad \text{for } \sigma_m = 170 \text{ MPa, and}$$

$$N_f = 7.6 x 10^{15} \sigma_a^{-5.0} \quad \text{for } \sigma_m = 260 \text{ MPa.}$$

32

*Endurance limit*

The endurance limits were determined by the staircase method using test sequences shown in Figs. 13 to 14. The resulting $10^7$ cycles endurance limit stresses were 82 MPa for $\sigma_m$ = 260 and 230 MPa for $\sigma_m$ = –200. The calculated standard deviation was in both cases less than half stress increment size. Therefore, the estimated standard deviations were rounded to 5 MPa for $\sigma_m$ = 260 MPa and to 12 MPa for $\sigma_m$ = –200 MPa.

Based on the S-N curves the endurance limit for $\sigma_m$ =170 MPa would be about 92 MPa, but this value was not specifically measured.
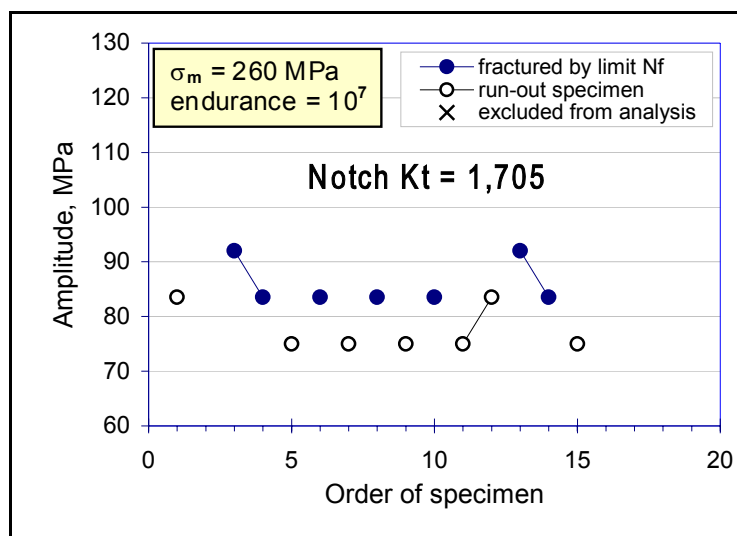


*Figure 13. Test sequence for endurance limit determination at 260 MPa mean stress.*
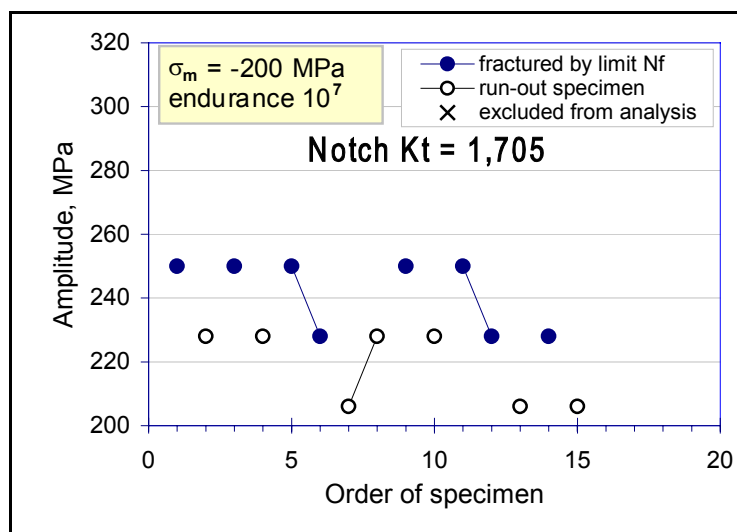


*Figure 14. Test sequence for endurance limit determination at –200 MPa mean stress.*

## 4.5  Notched specimens, variable amplitude

Variable amplitude testing has been performed on 30 notched test specimens. Tests lasting longer than $150 \cdot 10^6$ fatigue cycles were stopped even if failure did not occur. As with tests of smooth specimens, the cycles ratio, $n_{hc}$ / $n_{lc}$, has been chosen to maintain a nearly constant number of overloads per test. This results in a relatively constant proportion of damage caused by the overload cycles. The large cycles contributed only a small portion of the fatigue damage. Definitions of the terms for describing the variable amplitude loading are given in Fig. 2. The results are given in Table 18.

*Mean life S-N curves*

Variable amplitude notched specimen fatigue data is shown graphically in Fig. 15. Constant amplitude S-N lines from Fig. 12 are also shown in this figure. The best fit through the data points shown in Fig. 15 was determined using maximum likelihood estimation (MML) techniques and assuming an S-N relation

$$N_f = C\sigma_a{}^b \ .$$

The resulting equation for the variable amplitude loading data becomes

$$N_f = 8.6x10^{18}\sigma_a{}^{-6.7} .$$

It is worth of observing that the slope of the S-N curve for notched specimens remains quite constant far below the constant amplitude fatigue limit. Actually, data points at stress amplitudes of 97,4 and 68 MPa seem to follow very well the extrapolated S-N curve for constant amplitude loading. The combined data could also be fitted with a bi-linear S-N curve with the change in slope occurring somewhere around 60 MPa.

*Scatter in life*

The standard deviation in Log($N_f$) based on MML is 0.27 which is slightly less than that observed for smooth specimens but is greater than that observed for constant amplitude testing of notched specimens which was about 0.14. However, at a single stress amplitude the variable amplitude notched specimens had about the same degree of scatter as did the constant amplitude notched specimens.

*Table 18. Variable amplitude loading data of notched specimens.*

| Specim. code | low cycle | | high cycle | | Endurance to failure | | | |
|---|---|---|---|---|---|---|---|---|
| | $\sigma_{mean, lc}$ MPa | $\sigma_{a, lc}$ MPa | $\sigma_{mean, hc}$ MPa | $\sigma_{a, hc}$ MPa | $\frac{n_{hc}}{n_{lc}}$ | $N_f$ cycles | $n_{lc}$ blocks | run-out? |
| 1.11.13 | 168.5 | 158.5 | 259 | 68 | 20 000 | 6 770 800 | | |
| 1.11.14 | 168.5 | 158.5 | 259 | 68 | 20 000 | 1 982 100 | | |
| 1.11.15 | 168.5 | 158.5 | 259 | 68 | 20 000 | 5 051 900 | | |
| 1.11.16 | 168.5 | 158.5 | 259 | 68 | 20 000 | 6 082 500 | | |
| 1.9.27 | 168.5 | 158.5 | 259 | 68 | 20 000 | 2 651 800 | | |
| 1.9.28 | 168.5 | 158.5 | 259 | 68 | 20 000 | 8 308 500 | | |
| 1.9.29 | 168.5 | 158.5 | 259 | 68 | 20 000 | 2 476 000 | | |
| 1.8.17 | 168.5 | 158.5 | 259 | 68 | 20 000 | 6 013 700 | | |
| 1.8.18 | 168.5 | 158.5 | 259 | 68 | 20 000 | 7 781 100 | | |
| 1.8.19 | 168.5 | 158.5 | 259 | 68 | 20 000 | 6 578 100 | | |
| 1.11.17 | 183.2 | 173.2 | 259 | 97.4 | 3300 | 434 000 | | |
| 1.11.18 | 183.2 | 173.2 | 259 | 97.4 | 3300 | 889 900 | | |
| 1.11.19 | 183.2 | 173.2 | 259 | 97.4 | 3300 | 1 394 000 | | |
| 1.11.20 | 183.2 | 173.2 | 259 | 97.4 | 3300 | 676 900 | | |
| 1.8.20 | 183.2 | 173.2 | 259 | 97.4 | 3300 | 1 802 300 | | |
| 1.8.21 | 183.2 | 173.2 | 259 | 97.4 | 3300 | 1 147 200 | | |
| 1.8.22 | 183.2 | 173.2 | 259 | 97.4 | 3300 | 666 900 | | |
| 1.8.23 | 183.2 | 173.2 | 259 | 97.4 | 3300 | 551 800 | | |
| 1.9.25 | 183.2 | 173.2 | 259 | 97.4 | 3300 | 878 500 | | |
| 1.9.26 | 183.2 | 173.2 | 259 | 97.4 | 3300 | 1 396 400 | | |
| 1.11.21 | 159.4 | 149.4 | 259 | 49.8 | 300 000 | 67 047 000 | | |
| 1.11.22 | 159.4 | 149.4 | 259 | 49.8 | 300 000 | 72 503 000 | | |
| 1.11.23 | 159.4 | 149.4 | 259 | 49.8 | 300 000 | 60 015 000 | | |
| 1.8.37 | 159.4 | 149.4 | 259 | 49.8 | 300 000 | 49 949 000 | | |
| 1.8.38 | 159.4 | 149.4 | 259 | 49.8 | 300 000 | 26 762 000 | | |
| 1.8.39 | 159.4 | 149.4 | 259 | 49.8 | 300 000 | 99 501 000 | | |
| 1.8.40 | 159.4 | 149.4 | 259 | 49.8 | 300 000 | 133 200 000 | | **(R-O)** |
| 1.9.5 | 159.4 | 149.4 | 259 | 49.8 | 300 000 | 296 000 000 | | **(R-O)** |
| 1.9.6 | 159.4 | 149.4 | 259 | 49.8 | 300 000 | 52 603 200 | | |
| 1.9.7 | 159.4 | 149.4 | 259 | 49.8 | 300 000 | 53 001 000 | | |

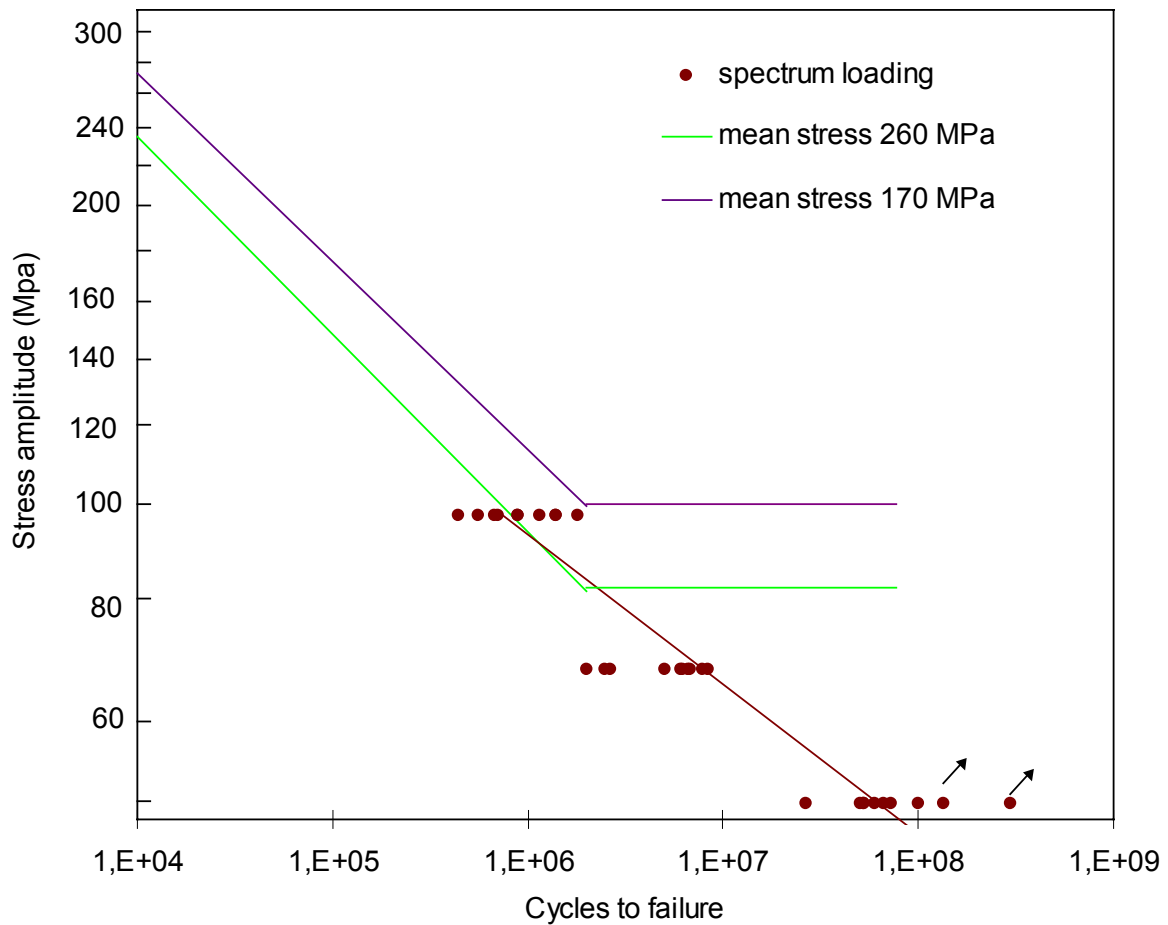**(R-O)** indicates run-outs, i.e., without failure interrupted tests

*Figure 15. Variable amplitude fatigue data for notched specimens.*

## 4.6  Bend specimens

Long-life fatigue data for the four point bending tests is given in Tables 19 to 21. The 20×20 mm cross section specimens were all taken from the same 200×200×300 mm ingot. These rectangular bars were intentionally taken from different portions of the casting to include quality variations in the test material. They were studied prior to fatigue testing to simulate different NDE methods as described later in this report. The fatigue data for these 20×20 mm cross section specimens is given in Table 19. Tables 20 and 21 show the fatigue data for the 10×10 mm and 40×40 mm cross section specimens, respectively.

Virtually all tests were performed using the same stress level, which allows statistical evaluation of the results. The discussion part of this report includes a statistical examination of the effects of both specimen size and the size of the ingot form which the specimens were taken. The variation of fatigue lives in the three bending test sets is described in Tables 19 to 21 and illustrated in Fig. 16.

The mean[13] lives and standard deviations at 250 MPa mean stress and 205 MPa stress amplitude are given in Tables 19 to 21. These values are given also for the case that the specimens containing clear defects are excluded. These scatter bands for nominally "defect free" material are marked in Fig. 16.

*Table 19. Four point bending data for 20×20 mm cross section specimens.*

| Specimen | $\sigma_{mean}$ | $\sigma_a$ | $N_f$ | comments |
|---|---|---|---|---|
| 2.1.03 | 250 | 205 | 75 062 | |
| 2.1.04 | *275* | *250* | *48 918* | note stress level |
| 2.1.05 | 250 | 205 | 65 078 | |
| 2.1.06 | 250 | 205 | 62 036 | |
| 2.1.11 | 250 | 205 | 123 360 | |
| 2.1.14 | 250 | 205 | 125 242 | |
| 2.1.18 | 250 | 205 | 76 321 | |
| 2.1.23 | 250 | 205 | 113 858 | |
| 2.1.28 | 250 | 205 | 104 372 | |
| 2.1.29 | 250 | 205 | 71 135 | |
| 2.1.36 | 250 | 205 | 105 570 | |
| 2.1.37 | 250 | 205 | 118 936 | |
| 2.1.83 | 250 | 205 | 122 183 | |
| 2.1.84 | 250 | 205 | 118 991 | |
| 2.1.85 | 250 | 205 | 119 786 | |
| 2.1.86 | 250 | 205 | 119 472 | |
| 2.1.93 | 250 | 205 | 129 028 | |
| 2.1.94 | 250 | 205 | 88 704 | |
| 2.1.95 | 250 | 205 | 35 846 | material defect |
| 2.1.96 | 250 | 205 | 32 314 | material defect |
| **whole set** | **250** | **205** | **89 000** | **geom. mean** |
| **defect free** | **250** | **205** | **99 000** | **geom. mean** |
| whole set | 250 | 205 | 1.5 | stand. deviation |
| defect free | 250 | 205 | 1.3 | stand. deviation |

---

[13] Geometric mean (mean in logarithmic scale) is used for $N_f$

*Table 20. Four point bending data for 10 x 10 mm cross section specimens.*

| Specimen | $\sigma_{mean}$ | $\sigma_a$ | $N_f$ | comments |
|---|---|---|---|---|
| 1.17.01 | 250 | 205 | 293 000 | |
| 1.17.02 | 250 | 205 | 287 000 | |
| 1.17.03 | 250 | 205 | 147 000 | |
| 1.17.04 | 250 | 205 | 445 000 | |
| 2.2.05 | 250 | 205 | 178 000 | |
| 2.2.06 | 250 | 205 | 94 000 | |
| 2.2.07 | 250 | 205 | 186 000 | |
| 2.2.08 | 250 | 205 | 175 000 | |
| 3.2.01 | 250 | 205 | 277 000 | |
| 3.2.02 | 250 | 205 | 341 000 | |
| 3.2.03 | 250 | 205 | 69 000 | material defect |
| 3.2.04 | 250 | 205 | 323 000 | |
| **whole set** | **(geometric mean &** | | **207 000** | **sd = 1.7** |
| **defect free** | **standard deviation)** | | **229 000** | **sd = 1.6** |

*Table 21. Four point bending data for 40 x 40 mm cross section specimens.*

| Specimen | $\sigma_{mean}$ | $\sigma_a$ | $N_f$ | comments |
|---|---|---|---|---|
| 1.19.01 | 250 | 205 | 345 500 | |
| 1.19.02 | 250 | 205 | 390 000 | |
| 1.19.03 | 250 | 205 | 334 200 | |
| 1.19.04 | 250 | 205 | 160 800 | |
| 2.2.01 | 250 | 205 | 114 400 | |
| 2.2.02 | 250 | 205 | 136 900 | |
| 2.2.03 | 250 | 205 | 170 100 | |
| 2.2.04 | 250 | 205 | 200 100 | |
| 3.1.01 | 250 | 205 | 558 700 | |
| 3.1.02 | 250 | 205 | 32 400 | material defect |
| 3.1.03 | 250 | 205 | 26 300 | material defect |
| 3.1.04 | 250 | 205 | 584 400 | |
| **whole set** | **(geometric mean &** | | **179 000** | **sd = 2.7** |
| **defect free** | **standard deviation)** | | **257 000** | **sd = 1.8** |
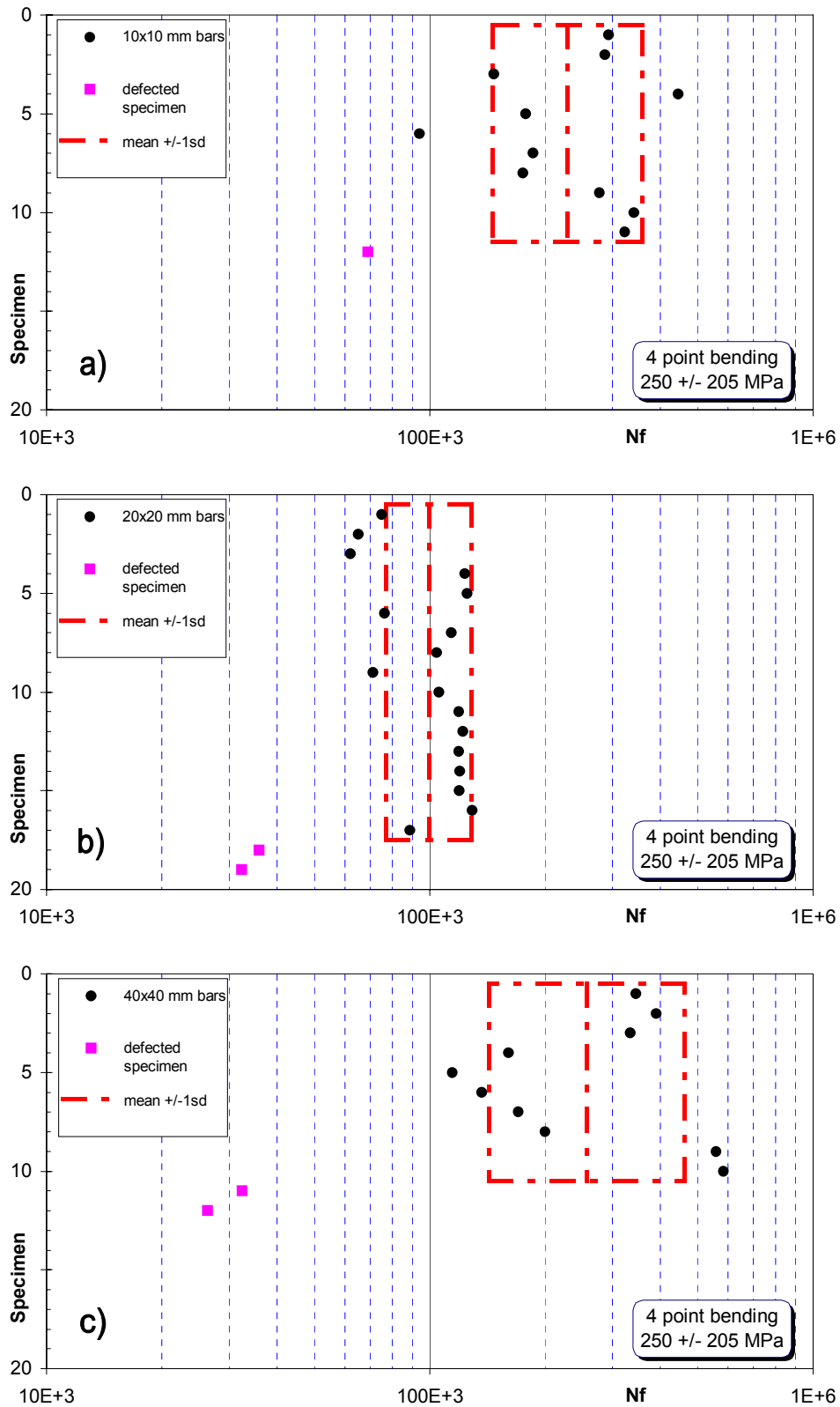
*Figure 16. Variation of fatigue lives in bending tests with σ*mean* = 250 Mpa and σ*a* = 205 Mpa. Specimen sizes: a) 10×10 mm ; b) 20×20 mm ; c) 40×40 mm.*

It should be noted that all 20ˣ20 mm specimens were taken from the large 200ˣ200 mm ingots which seem to have lower fatigue strength than the others. The 10ˣ10 mm and 40ˣ40 mm specimens were taken from ingots of all sizes, which explains the observed larger scatter for the 10ˣ10 mm and 40ˣ40 mm data.

# 4.7 Torsion fatigue

A small task investigating torsion fatigue properties of GRP 500 was performed. The test parameters and data is given in Tables 22 to 24.

Torsion is particularly useful for observing the changes in fatigue damage accumulation for materials. In fully reversed torsion the observed endurance limit is about 183 MPa (Tables 23, 24), while the endurance limit is about 125 MPa for R = 0 torsion loading (Table 22). Data from Tables 23 and 24 is presented graphically in Fig. 17.

The endurance limit in torsion is about 80% of the endurance limit in tension. The limited amount of finite life data shows a similar reduction. This indicates that, even though the failure mechanism for GRP is along principal stress planes, maximum principal stress alone cannot be used to correlate torsion and tension data for this material. The allowable endurance limit stress in torsion is one aspect of the universal design curve for GRP, which is outlined later in this report and presented in Appendix 3.

*Table 22. R = 0 torsion testing of tubular specimens. Preliminary test series with specimen gauge section outer and inner diameters 25 and 20 mm.*

| Specimen | $F_{max}$ (kN) | T (n-m) | $\tau_{mean}$ (MPa) | $\tau_a$ (MPa) | $N_f$ (cycles) | Comments |
|----------|------|---------|------------|---------|------------|------------|
| 1.5.01 | 12 | 420 | 116 | 116 | 1 265 000 | |
| 1.5.02 | 12 | 420 | 116 | 116 | 8 600 000 | no failure |
| 1.5.02* | 14 | 490 | 135 | 135 | 409 000 | |
| 1.5.03 | 14 | 490 | 135 | 135 | 373 000 | |
| 1.5.04 | 12 | 420 | 116 | 116 | 20 000 000 | no failure |
| 1.5.04* | 14 | 490 | 135 | 135 | 1 016 000 | |

* indicates re-testing of a previous non-failed specimen

*Table 23. R = −1 torsion testing of tubular specimens with gauge section outer and inner diameters 23.8 and 19.5 mm.*

| Specimen | $F_{max}$ (kN) | T (n-m) | $\tau_{mean}$ (MPa) | $\tau_a$ (MPa) | $N_f$ (cycles) | Comments |
|---|---|---|---|---|---|---|
| 1.10.2 | 7 | 245 | 0 | 168,5 | 2 000 000 | no failure |
| 1.10.3 | 8 | 280 | 0 | 192,5 | 182 000 | |
| 1.10.4 | 7.6 | 266 | 0 | 183 | 1 400 000 | |
| 1.20.1 | 7.6 | 266 | 0 | 183 | 2 300 000 | no failure |
| 1.9.3 | 7.6 | 266 | 0 | 183 | 2 000 000 | no failure |
| 1.9.4 | 7.6 | 266 | 0 | 183 | 1 241 000 | |
| 1.17.5 | 7.6 | 266 | 0 | 183 | 1 038 523 | |
| 1.15.3 | 7.6 | 266 | 0 | 183 | 2 100 000 | no failure |
| 1.15.4 | 7.6 | 266 | 0 | 183 | 2 200 000 | no failure |

*Table 24. R = −1 torsion testing of tubular specimens with added multiaxial stresses. Specimen gauge section outer and inner diameters 23.8 and 19.5 mm.*

| Specimen | $F_{max}$ (kN) | T (n-m) | $\tau_{mean}$ (MPa) | $\tau_a$ (MPa) | $N_f$ (cycles) | Comments |
|---|---|---|---|---|---|---|
| 1.9.1 | 7.6 | 266 | 0 | 183 | 487 966 | |
| 1.9.2 | 7.6 | 266 | 0 | 183 | 1 082 102 | |
| 1.15.1 | 7.6 | 266 | 0 | 183 | 1 284 220 | |
| 1.15.2 | 7.6 | 266 | 0 | 183 | 1 068 410 | |
| 1.17.6 | 7.6 | 266 | 0 | 183 | 1 430 988 | |
| 1.11.1 | 7.45 | 245 | 0 | 179 | 2 000 000 | no failure |
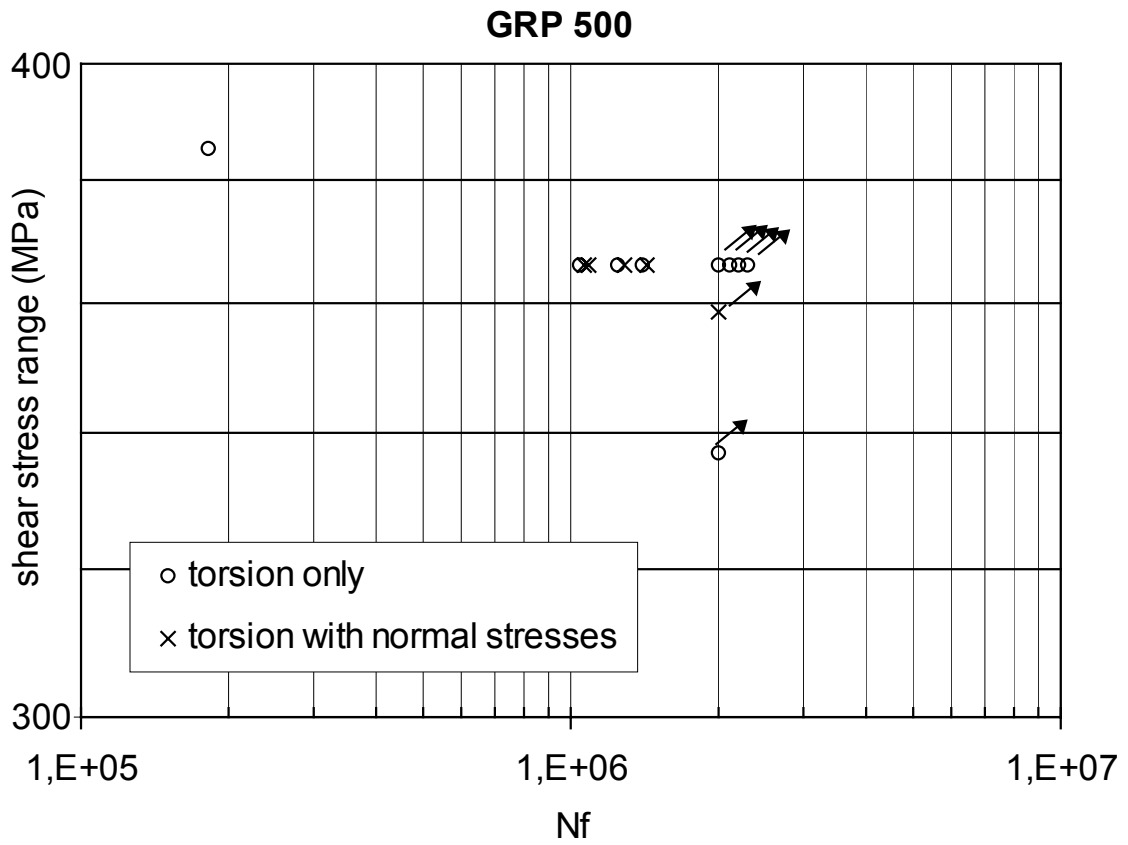
*Figure 17. Fully reversed torsion fatigue of GRP 500; data from Tables 23 and 24. Note that Y scale gives shear stress ranges =* $\tau_{max} - \tau_{min} = 2 \cdot \tau_a$ .

# 5. Damage mechanisms and defects

## 5.1 Microstructure and fatigue initiation sites

GRP 500 has a very complex microstructure comprised of iron matrix containing ferrite and pearlite, spheroidal graphite nodules and micro-pores. Typical microstructures for a 500 MPa ultimate strength and 600 MPa ultimate strength irons are shown in Fig. 18. The material shown in Fig. 18a) was taken from a Wärtsilä 64 cylinder head while that shown in Fig. 18b) was taken from a 100×100×300 mm cast ingot.
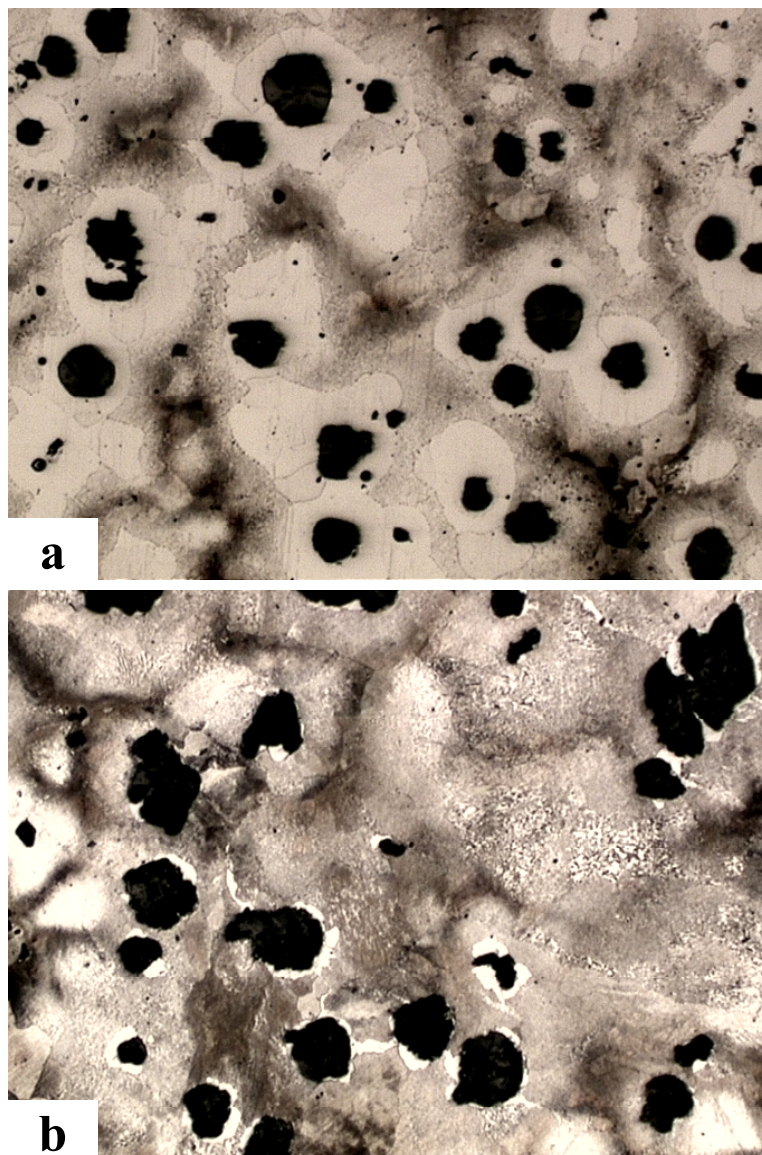


*Figure 18. Microstructures of nodular iron. a) Wärtsilä 64 cylinder head (500 MPa); b) for this study cast ingot (600 MPa). The measured ultimate strengths in parthesis.*

Examination of fracture surfaces for specimens cycled just above the endurance limit showed that fatigue failure is normally dominated by the nucleation and growth of individual cracks from shrinkage pores just below the specimen surface. At stress levels near the endurance limit, numerous micro-cracks are initiated but failure is dominated by the propagation of a single crack. Crack coalescence does not play an important role.

Shrinkage pores several hundred microns in diameter are a common feature of thick section castings such as the ingots in this investigation. The graphite nodules characteristic of this material were significantly smaller with diameters in the range of 30 - 60 microns. Exceptional large graphites and magnesium rich inclusions were of a size similar to the shrinkage pores. In some specimens failure initiated at these magnesium rich inclusions or exceptionally large graphites.

Fig. 19 shows examples of the most common types of fatigue initiation sites for GRP 500. Fig. 19a) represents the most common type, a shrinkage pore, Fig. 19b) shows a typical MgS inclusion.

*Distribution of fatigue initiation sites*

The sizes and distribution of the defects will vary depending on production parameters and geometry of the casting. Fig. 20 shows the distribution of most severe defects observed in fatigue specimens taken from both the Wärtsilä 64 cylinder head (batch 1) and from the 100×100×300 mm ingots (batch 2). Fig. 20 represents an extreme value distribution plot of the most severe defects observed.

The steeper line corresponding to batch 2 material indicates less statistical variation in defect size leading to smaller scatter in the observed fatigue limit. The fact that the line for batch 2 material is also to the left of the line for batch 1 material indicates a smaller mean size of defects, which explains the higher mean fatigue strength of that material. However, due to complex microstructure, defects are only one factor influencing the fatigue strength. For example, the strength of the matrix material surrounding the potential initiator defects is also important.

*The Murakami-Endo model for fatigue strength*

The fatigue mechanisms and models for predicting fatigue endurance limit for nodular iron was studied in a MSci thesis by Laura Taivalaho. The $\sqrt{area}$ geometrical parameter model developed by Murakami and Endo is very practical and shown to be widely applicable. Originally it was developed for high strength steel, but it has been applied to nodular cast iron as well (Murakami 1996, Beretta et al. 1997).
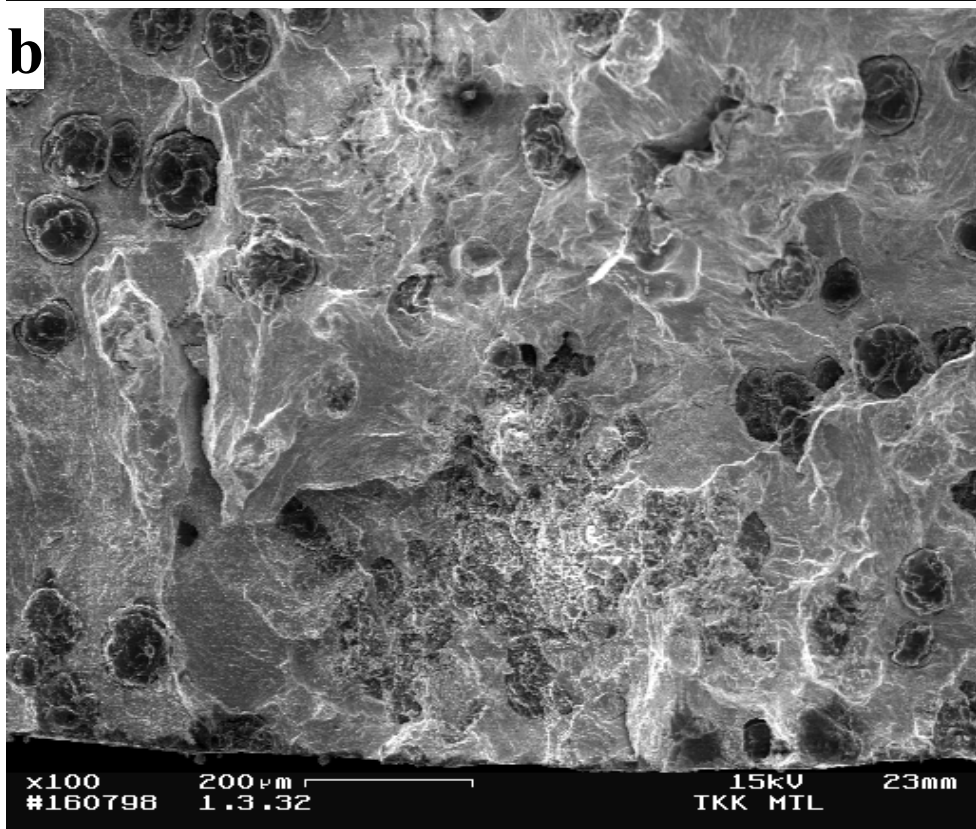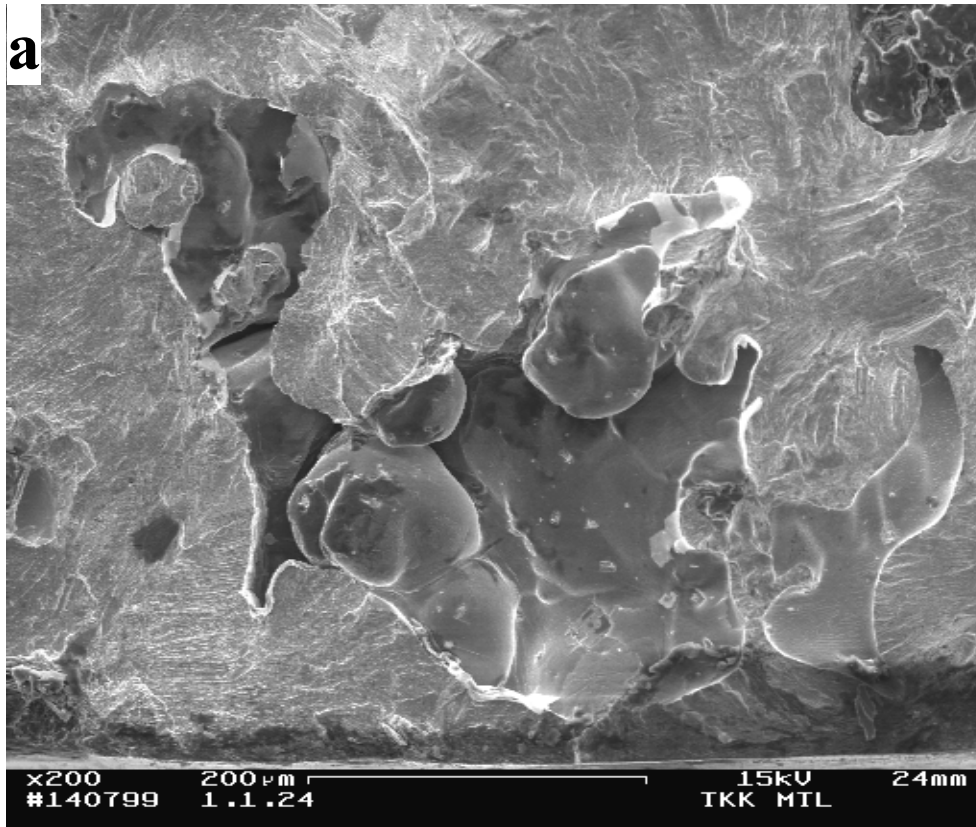
*Figure 19. Examples of defects leading to failures: a) shrinkage pore ;  b) inclusion.*

According to the model the key elements are the size of the initiating inclusion, porosity or graphite and the hardness of the matrix. Also location of the initiator has an effect. Defects just below the surface are most severe.

In brief, we can say that the observations within the current project, especially concerning the role of defects on fatigue strength, are in good agreement with the Murakami-Endo Model. Some concerns were raised about definition of the matrix hardness value for the dual phase ferritic-pearlitic metal matrix. The model might be more straightforward applicable to pure ferritic or pearlitic iron grades. Those who are interested in more details of this part of the project, are adviced to read the thesis (Taivalaho 1999).
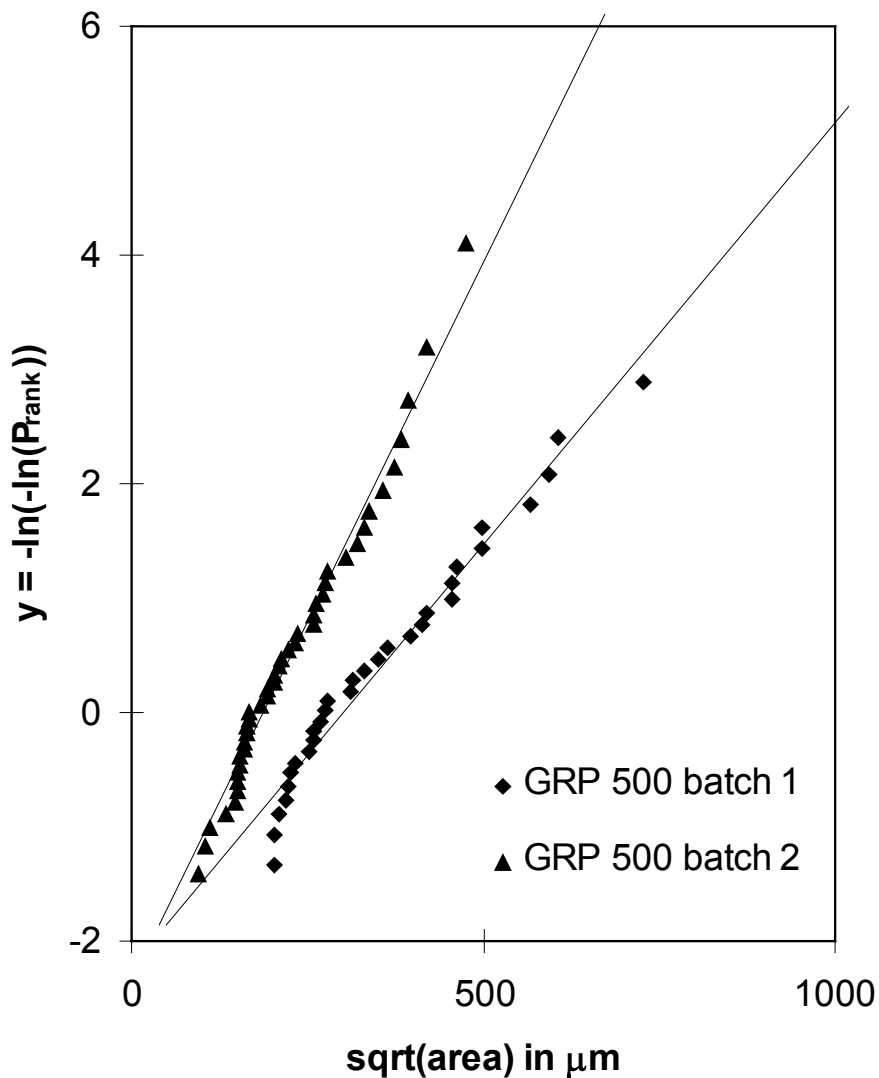


Figure 20. Distribution of most severe defects observed in GRP 500 test specimens.

## 5.2 Growth of micro-cracks

It is worth of noting that the fatigue limit of this nodular iron is not controlled by crack "initiation", but rather by growth of micro-cracks. A lot of non-propagating cracks were observed in specimens loaded at stress amplitudes just above or below the fatigue limit.

Fatigue life of structural steels is dominated by nucleation and growth of cracks on shear stress planes. As stress level decreases the number of nucleated cracks also decreases so that at long lives fatigue of structural steels is dominated by nucleation and growth of single cracks. In structural steels propagation along mode I planes begins relatively late in life. This is in contrast to the behaviour of the nodular cast iron, where fatigue occurs through crack propagation along mode I planes perpendicular to the primary stress axis.

Fig. 21 shows the small crack behaviour of GRP 500 under cyclic torsion loading. Cracks nucleate and propagate on planes oriented at approximately ±45°. Final failure for all GRP 500 torsion specimens was the result of spiral cracks around the specimen. This confirms that fatigue failure of the nodular iron is dominated by mode I crack growth. Locally the crack pattern is very tortuous as the crack propagates through graphite nodules, shrinkage pores and inclusions. By contrast, the small crack behaviour of C45 structural steel under torsion loading is different. The cracks grow along shear planes oriented at 0° and 90° angles as seen in Fig. 22.

Because of the difference in damage accumulation mechanism, fatigue models and design rules for structural steels will not necessarily work for nodular irons. This problem is discussed further by Marquis and Socie (1999).
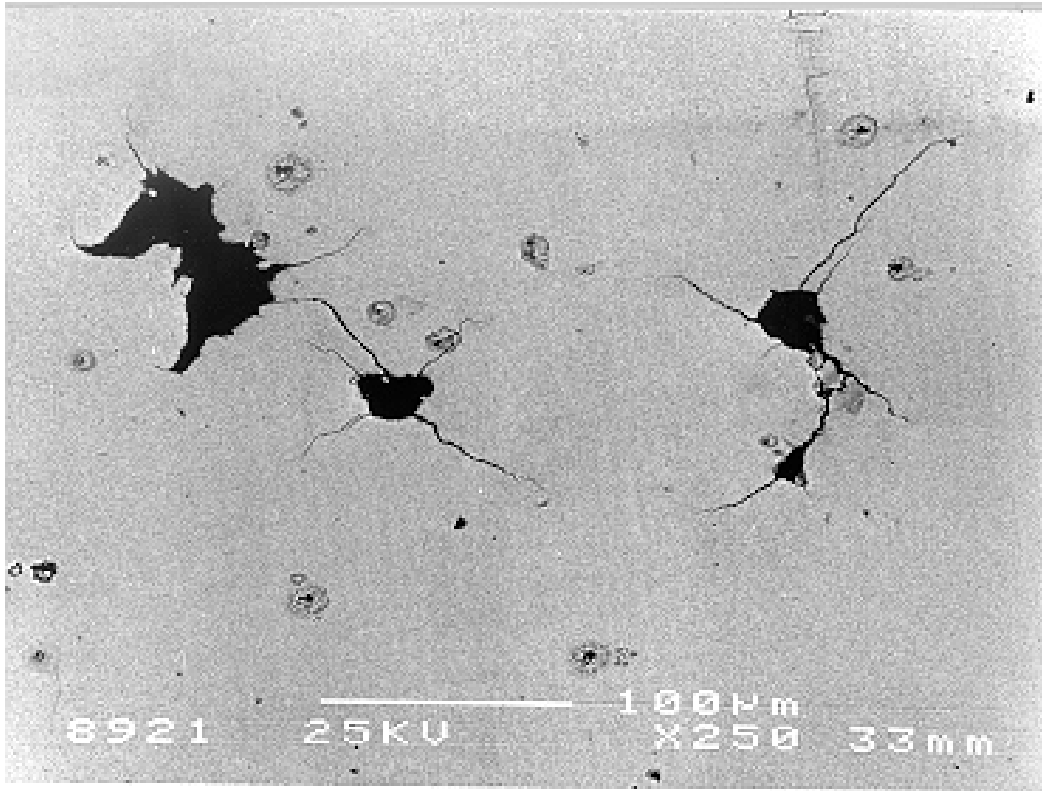
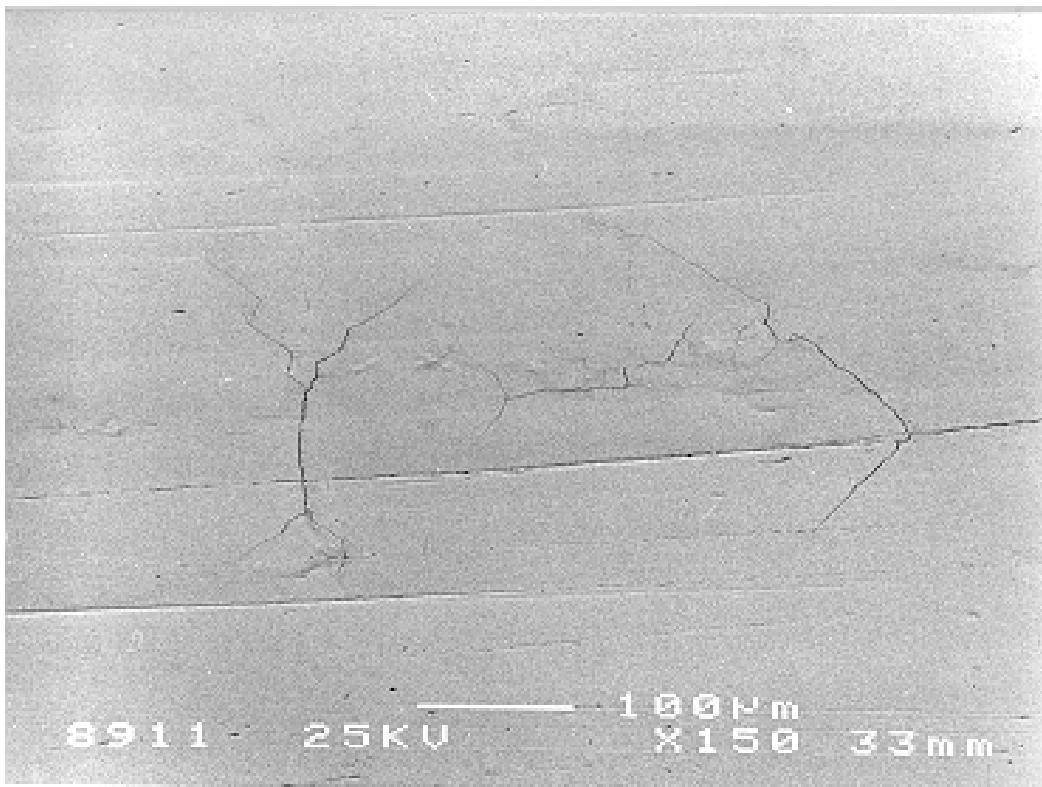*Figure 21. Crack nucleation and propagation for GRP 500 in torsion fatigue loading.*



*Figure 22. Crack nucleation and propagation for C45 steel in torsion fatigue loading.*

48

## 5.3 NDT and fatigue strength

In order to study the possibilities for correlating the non-destructive testing (NDT) results to fatigue strength, detailed studies were performed both for acceptable quality material and for defected material.

*Normal quality castings*

Detailed ultrasound measurements were performed prior to fatigue testing to simulate different NDT methods on 20 specimens taken from a single 200x200x300 mm ingot. The specimens were taken from different portions of the ingot to try to correlate the ultrasound propagation and fatigue test results to small variations in the microstructure.

Ultrasound velocity and attenuation both through the specimen and along the surface layers were measured in different orientations. A scanning acoustic microscope (SAM) was used and ultrasound propagation maps were produced of the 60x20x20 mm mid sections of the rectangular 195 mm long specimens.

Locations within the ingot and fatigue lives for these specimens were shown earlier in this report, see Fig. 4 and Table 19. Results of the hardness and ultrasonic SAM measurements are summarised in Table 25. Some variations of properties within the ingot could be detected by the SAM. For example, from the SAM results calculated material density correlated quite well with the physically measured density. The most prominent difference was a hardness gradient within the specimens 3 to 6. These four specimens had also the highest C-scan[14] results and three of them had short fatigue lives. One of them was tested on a higher stress level.

As expected, the shortest fatigue lives were measured for specimens taken from the top of the ingot. One specimen had a notable defect, which was clearly revealed by the SAM, Fig. 23. This defect resulted into to the shortest life. A pore larger than one mm in size was found at the fracture surface. The other specimens did not contain any significant defects, which prevented direct comparison of NDT and fatigue test results. However, some trends in ultrasound measurements and fatigue strength could be seen.

---

[14] C-scan is a planar image of the studied sample obtained by focused ultrasonic measurements.

*Table 25. Ultrasonic microscopy results for 20 ×20 mm bars. Hardness is average of three measurements near the bottom (A) and at the upper end of the specimen (B). Average ultrasound velocity for longitudinal, shear and surface waves in different orientations (S1, S2, S3) is given in meters per second. Attenuation of longitudinal waves is given in dB/40 mm and attenuation of Rayleigh surface waves in an arbitrary unit (100mV/5mm). The percentage of area exceeding a set threshold criteria is obtained from C-scan images (see Fig. 23).*

| Sample block; location | Hardness HB | | Velocity, m/s | | | | | | | Attenuation | | | C-scan % area |
|---|---|---|---|---|---|---|---|---|---|---|---|---|---|
| | | | Longit. | | Shear | | | Rayleigh | | Longit. | | Rayl. | |
| | A | B | S1 | S2 | S1 | S2 | S3 | S2 | S3 | S1 | S2 | S2 | 100-X |
| 2.1.03 | 207 | 156 | 5660 | 5668 | 3083 | 3111 | 3032 | 2721 | 2729 | 30 | 28 | 23,0 | 99,7 |
| 2.1.04 | 201 | 168 | 5666 | 5657 | 3067 | 3109 | 3045 | 2752 | 2723 | 30 | 30 | 23,0 | 99,7 |
| 2.1.05 | 207 | 162 | 5663 | 5660 | 3071 | 3116 | 3032 | 2753 | 2737 | 29 | 27 | 29,6 | 99,2 |
| 2.1.06 | 201 | 163 | 5654 | 5654 | 3068 | 3113 | 3056 | 2718 | 2726 | 28 | 28 | 28,4 | 99,8 |
| 2.1.11 | 201 | 201 | 5676 | 5655 | 3061 | 3070 | 3032 | 2729 | 2710 | 32 | 28 | 25,6 | 96,9 |
| 2.1.14 | 201 | 201 | 5670 | 5669 | 3076 | 3098 | 3030 | 2726 | 2739 | 28 | 26 | 21,6 | 98 |
| 2.1.18 | 201 | 201 | 5618 | 5651 | 3071 | 3060 | 3032 | 2723 | 2710 | 32 | 29 | 22,8 | 94,3 |
| 2.1.23 | 201 | 201 | 5661 | 5661 | 3093 | 3071 | 3022 | 2747 | 2721 | 30 | 25 | 20,2 | 97,6 |
| 2.1.28 | 201 | 201 | 5722 | 5699 | 3108 | 3081 | 3018 | 2688 | 2721 | 27 | 30 | 24,6 | 97,4 |
| 2.1.29 | 201 | 201 | 5692 | 5702 | 3077 | 3105 | 3020 | 2721 | 2696 | 30 | 29 | 25,6 | 97,8 |
| 2.1.36 | 197 | 200 | 5690 | 5680 | 3072 | 3077 | 3031 | 2696 | 2745 | 28 | 30 | 24,6 | 98,8 |
| 2.1.37 | 197 | 201 | 5677 | 5688 | 3071 | 3070 | 3032 | 2737 | 2729 | 30 | 30 | 25,6 | 98,7 |
| 2.1.83 | 201 | 201 | 5678 | 5665 | 3081 | 3088 | 3022 | 2699 | 2712 | 30 | 31 | 23,2 | 97 |
| 2.1.84 | 201 | 200 | 5676 | 5698 | 3094 | 3075 | 3035 | 2715 | 2721 | 30 | 30 | 25,6 | 96,7 |
| 2.1.85 | 201 | 201 | 5667 | 5688 | 3087 | 3103 | 3035 | 2721 | 2723 | 31 | 31 | 23,6 | 96,9 |
| 2.1.86 | 201 | 201 | 5672 | 5679 | 3084 | 3080 | 3030 | 2723 | 2731 | 30 | 30 | 24,4 | 96,6 |
| 2.1.93 | 197 | 197 | 5649 | 5665 | 3104 | 3113 | 3035 | 2696 | 2715 | 31 | 30 | 23,6 | 98,8 |
| 2.1.94 | 200 | 200 | 5639 | 5665 | 3096 | 3105 | 3028 | 2753 | 2704 | 32 | 27 | 24,0 | 98,8 |
| 2.1.95 | 201 | 201 | 5659 | 5658 | 3107 | 3105 | 3031 | 2702 | 2737 | 31 | 31 | 23,2 | 99 |
| 2.1.96 | 200 | 200 | 5648 | 5669 | 3103 | 3114 | 3055 | 2712 | 2739 | 31 | 30 | 23,6 | 98,5 |

The average longitudinal or Rayleigh wave velocity and attenuation did not notably correlate with fatigue strength. This may be explained by the fact that the local weakest link defect does not necessary correlate with the small differences in the nominally good quality material's average properties. However, the area of reduced velocity, as determined from the C-scans, correlated with the fatigue strength, Fig. 24a. For some unknown reason, also the average shear wave velocity seems to correlate with the fatigue strength, Fig. 24b.

In this preliminary study we could note that mechanised ultrasonic testing would be able to detect and localise defects which are smaller than the current acceptance criteria for NDT. Ultrasonic measurements were also capable of finding variations even in nominally defect-free material, but the potential for refined fatigue resistance predictions in practical applications still remains unclear. Further studies – preferably with larger variation of test material quality – would be needed to explain the observations and to assess the applicability of NDT in fatigue life prediction. Further work in this area should be pursued.
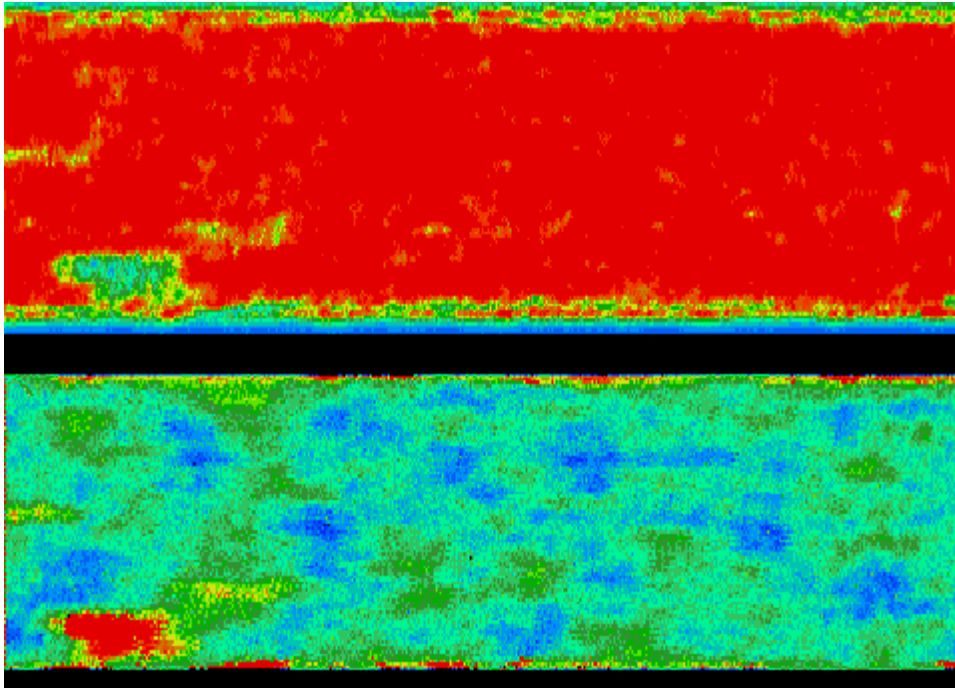
*Figure 23. Longitudinal and shear wave velocity based C-scan plots of specimen 2.1.96, which had the shortest fatigue life. The failure initiated from a more than 1 mm large defect seen as a prominent indication near the lower surface in the left of the scanned section. The scanned area is 60 x 20 mm.*
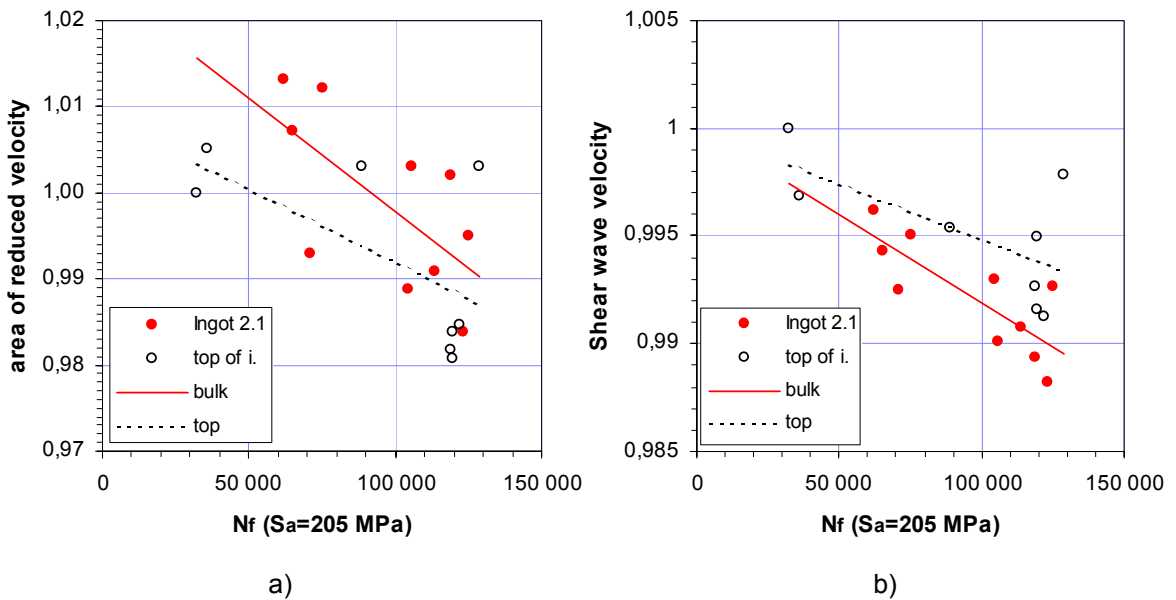


a)                                                      b)

*Figure 24. Correlation of measured fatigue life ($N_f$) and NDT data: a) C-scan based on sound velocity, b) Across the specimen measured shear wave velocity as average of measurements in three orientations. The NDT results are normalised to the value of the shortest life specimen 2.1.96.*

*Castings with defects*

The previous NDE measurements focussed primarily on specimens that were considered defect free. Therefore, the differences in both ultrasonic and fatigue testing were small. To get a more realistic picture of the currently used NDT acceptance criteria, it was decided to test also GRP with known defects.

Large defects are occasionally detected as part of the normal quality control procedure. They would not be permitted in the highly stressed areas of a structure, but by quantifying the negative impact of these defects, rational decisions could be made on how large defects could be allowed in less highly stressed areas.

Four 50ˣ200ˣ300 mm ingots were found to have defects which exceeded the $\varnothing$5 mm acceptance curve. Detailed inspection reports for these ingots are given in Appendix 1. After inspection the bars were cut into four-point bend test specimens according to Fig. 7, except that the span width was 45 mm for the inner span and 115 mm for the outer span. During fatigue loading the side of the bar containing the largest defects was subjected to tensile loading.

The obtained fatigue data is presented numerically in Table 26.

*Table 26. Bending fatigue data for 20ˣ20 mm  specimens with known large defects.*

| Specimen | $\sigma_{mean}$ (MPa) | $\sigma_a$ (MPa) | $N_f$ | Comments |
|----------|------------------------|-------------------|-----------|----------|
| 3.2.01 | 183 | 150 | 104 000 | |
| 3.2.02 | 183 | 150 | 111 000 | |
| 3.3.01 | 183 | 150 | 143 000 | |
| 3.4.01 | 183 | 150 | 81 000 | |
| 3.5.01 | 183 | 150 | 285 000 | |
| 3.2.03 | 130 | 106 | 369 000 | |
| 3.3.02 | 115 | 94 | 174 000 | |
| 3.4.02 | 101 | 83 | 1754 000 | |
| 3.5.02 | 101 | 83 | 1115 000 | |
| 3.5.03 | 101 | 83 | 1943 000 | |
| 3.2.04 | 101 | 83 | 1855 000 | |
| 3.3.03 | 101 | 83 | 905 000 | |
| 3.2.05 | 101 | 83 | 5850 000 | |
| 3.2.04 | 101 | 83 | 768 000 | |
| 3.4.03 | 101 | 83 | 1090 000 | |

The fatigue data for defected material from Table 26 is shown graphically in Fig. 25 together with the S-N curve estimated for the defect free material. The fatigue limit stress for the specimens with defects was about half of the fatigue limit for the defect free material. As expected, the S-N curve was also much steeper, indicating that these large defects very quickly started to behave as long cracks.
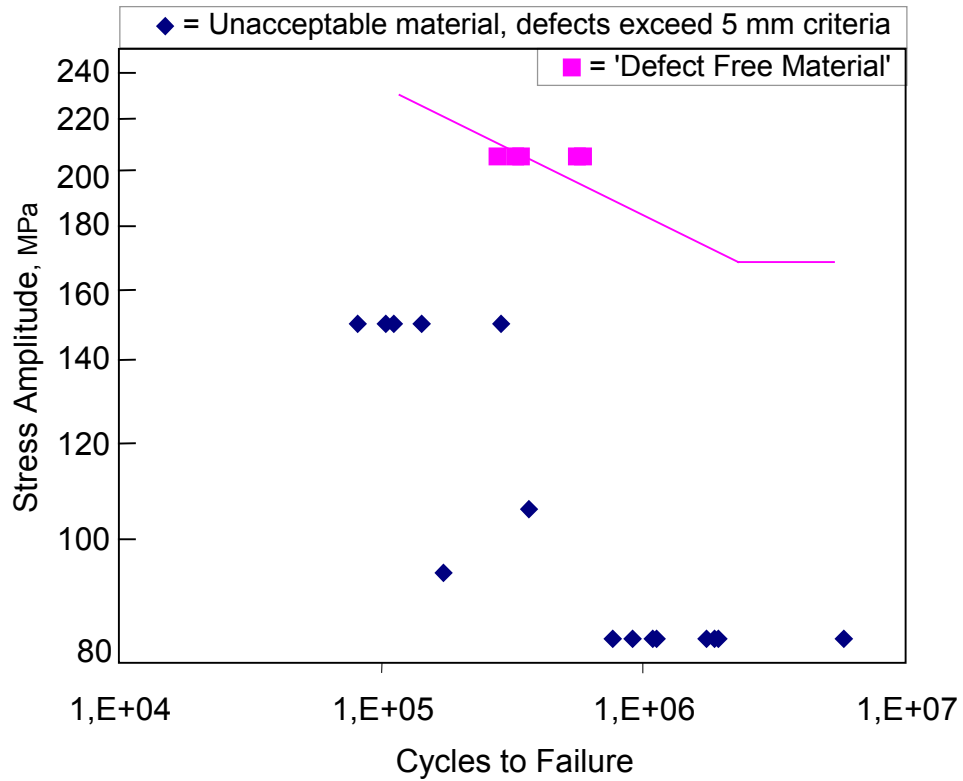


*Figure 25. Bending fatigue data for specimens with large defects.*

Fracture surfaces for three sample specimens are shown in Fig. 26. They show multiple defects ranging in size from several millimetres to about 15 mm in diameter.

*Figure 26. Fracture surfaces for defect containing specimens 3.4.01, 3.3.01 and 3.2.01.*

# 6. Universal fatigue curve for nodular iron

A revised form of the Haigh diagram for nodular cast irons has been proposed as part of this study. The model takes into account material static strength, stress ratio, stress state (torsion or uniaxial), and specimen size effects. This has been verified for nodular iron with ultimate strength between 500 and 600 MPa and for many different stress ratios, stress states and specimen geometries.

The principle of the universal fatigue curve for nodular iron is illustrated in Figs. 27 and 28. Fig. 27 shows the large amount of scatter observed in a the Haigh diagram for nominally identical material depending on the specimen type, component size, loading mode and material static properties.

Insight into the mechanism of fatigue failure has led to proposing the universal fatigue curve shown in Fig. 28. All data falls along a single design line when this revised form of the Haigh diagram is used.
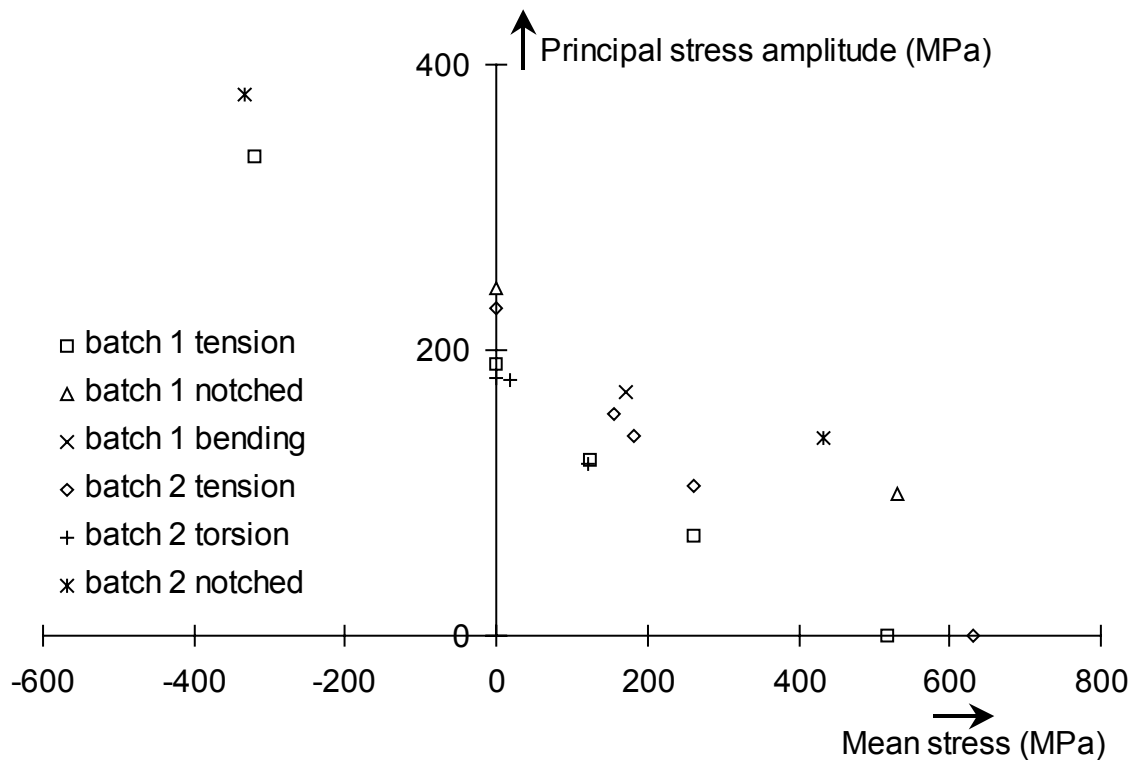


*Figure 27. Data from 16 series of fatigue tests on nodular cast iron with 500 - 600 Mpa ultimate strength plotted on a Haigh diagram. Note that each point represents approximately 15 long-life test series.*
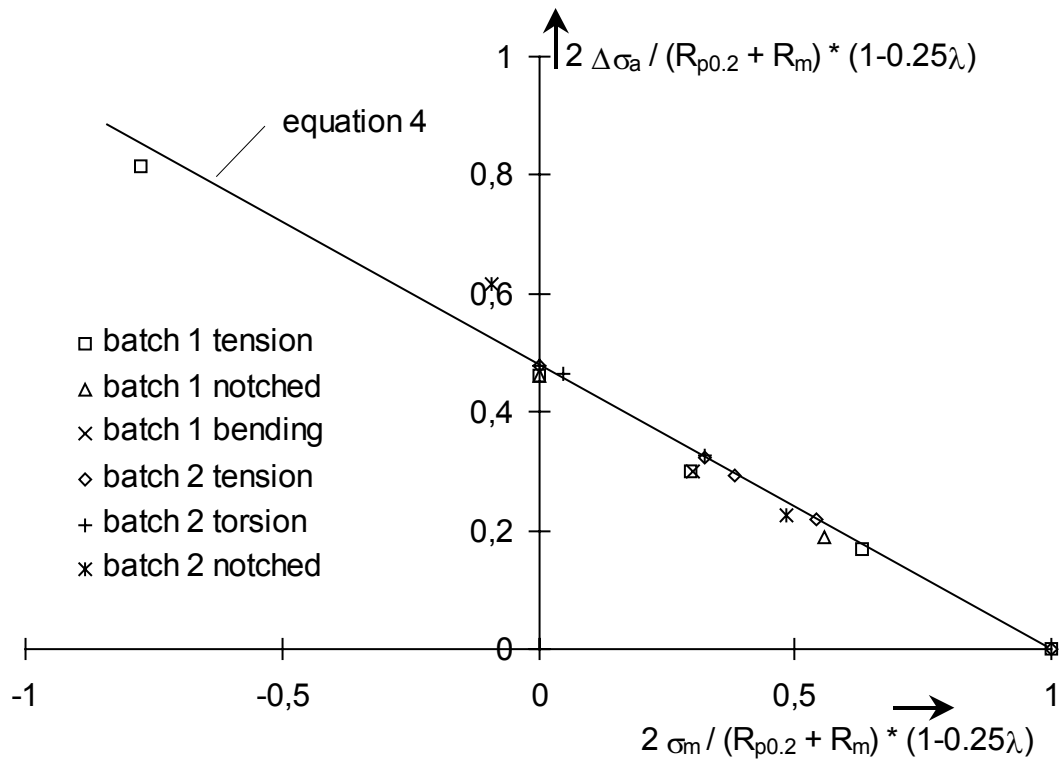
*Figure 28. Same data as in Fig. 27 plotted on the proposed universal fatigue curve for GRP. Corrections are made for material strength, stress state, and statistical size effect. $R_m$ = ultimate strength, $R_{p0,2}$ = yield strength, and $\lambda$ = biaxial stress ratio ($\sigma_2$ / $\sigma_1$).*

# 7. Discussion

## 7.1 Size effects in bending tests

Virtually all bending fatigue tests were performed using the same stress level, which allows statistical examination of the effects of both specimen size and the size of the ingot form which the specimens were taken. Figs. 29 and 30 show the probability of failure vs. $\log(N_f)$ for the specimens. Three results from specimens containing known defects and one specimen tested at a higher stress level are excluded from these figures.

**based on ingot size**
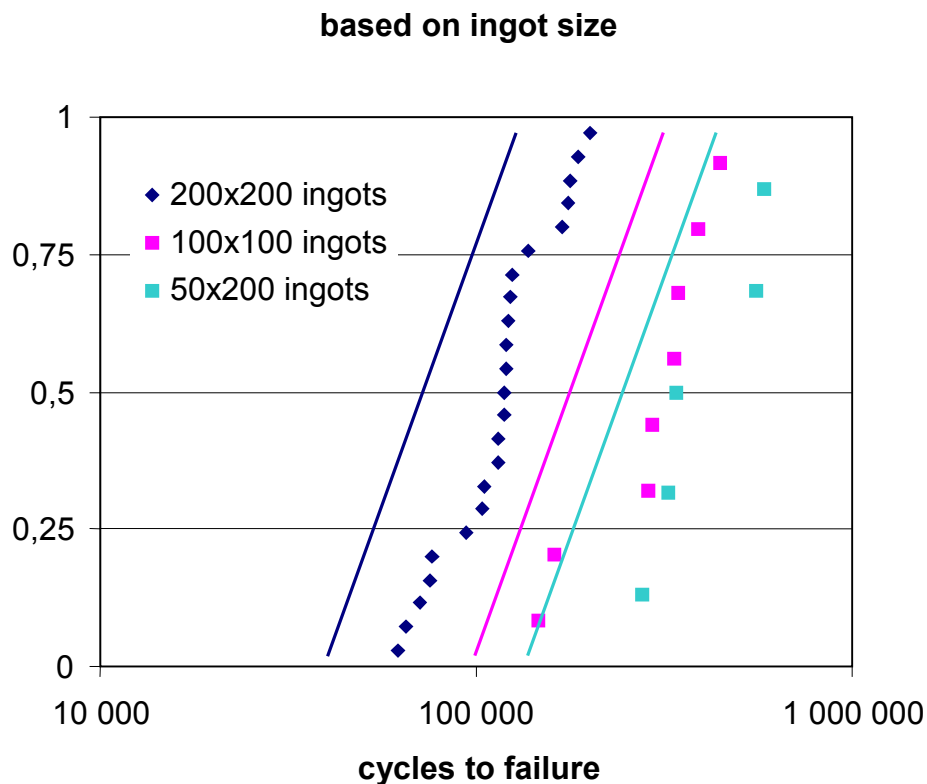


*Figure 29. Fatigue strength of four-point bend specimens taken from ingots of different sizes; $\sigma_a$ = 205 MPa, R = 0.1.*

### Influence of ingot size

Fig. 29 shows the fatigue strength distribution as a function of the size of the ingot from which the specimens were taken. The specimens taken from the largest ingots were clearly the weakest set from a fatigue point of view. The fatigue life increased as the wall thickness decreased. The curves in Fig. 29 have the same slope indicating that the standard deviation of logarithmic fatigue life remains constant although the mean life is changed.

Based on the fatigue life differences in Fig. 29 and the slope on the S-N curves, it appears that the fatigue strength of the material taken from the 50ˣ200ˣ300 ingots would be approximately 25% greater than the fatigue strength of the material taken from the 200ˣ200ˣ300 ingot. Static tensile test series for the other ingots should be performed to allow comparison of the size effects in monotonic and cyclic properties.

**based on specimen size**
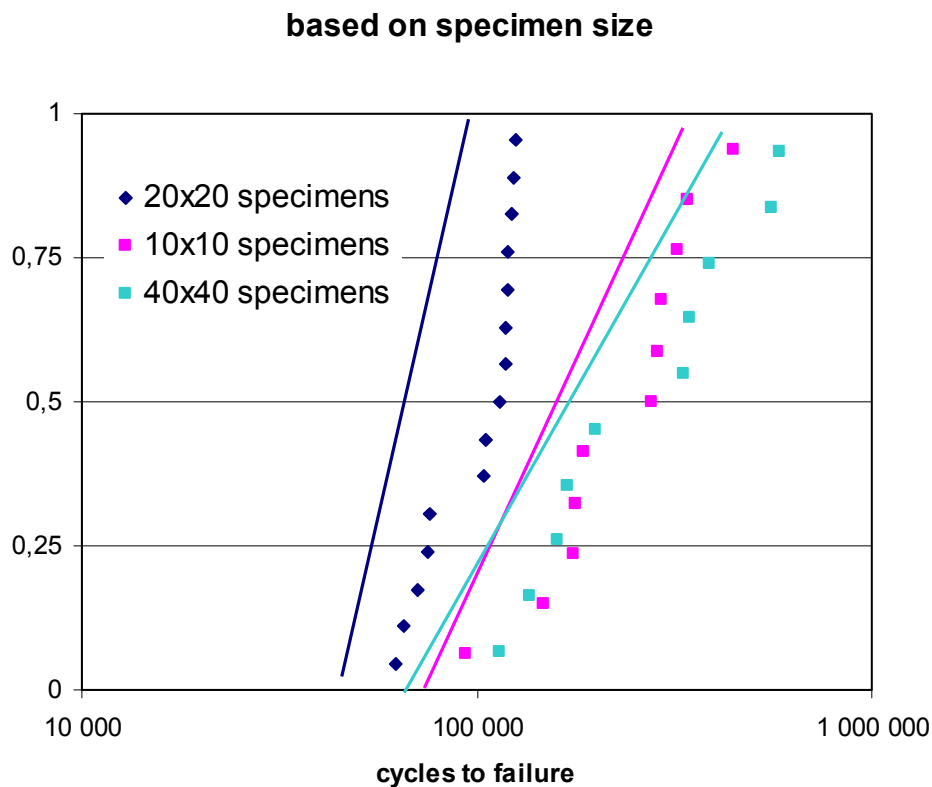


*Figure 30. Fatigue strength of four-point bend specimens of three different sizes; $\sigma_a = 205$ MPa, R = 0.1*

### *Influence of specimen size*

Fig. 30 shows the fatigue strength distribution as a function of bend specimen cross section. There appears to be no difference between the smallest and largest specimens (10ˣ10 mm and 40ˣ40 mm). No specimen size or stress gradient effects are seen here. But the intermediate size 20ˣ20 mm specimens have clearly shorter lives – or lower strength – and steeper slope, i.e., smaller scatter.

It should be remembered that all the 20ˣ20 mm specimens were taken from the 200ˣ200 mm ingots which seem to have lower strength (see Fig. 29). On the contrary, the 10ˣ10 mm and 40ˣ40 mm specimens were taken from ingots of all sizes. This also explains the observed larger scatter for the 10ˣ10 mm and 40ˣ40 mm data.

According to the weakest link theory, the 10x10 mm specimens would have approximately 7% greater fatigue strength than the 40x40 mm specimens. Assuming an S-N slope of −5, this should result in fatigue lives about 40% longer for the 10x10 mm specimens, which was not observed. But it should be noted that 40% difference in life on an S-N curve is still fairly small. The scatter in the data, primarily due to the different ingot sizes seems to dominate and hides the small differences expected due to specimen size.

## 7.2  Influence of loading mode

The majority of bend specimens were tested with a mean stress of 250 MPa and an amplitude of 205 MPa. Average fatigue life for specimens taken from the 100x100 mm ingots was about 200 000 cycles. According to Eq. 2 an axial specimen tested with the same mean stress would last the same number of cycles only by reducing the stress amplitude to about 145 MPa. The permitted amplitude in axial tension, therefore, is only 70% of the allowed amplitude in bending. This is equal to the 70% rule often used to relate bending fatigue data to axial fatigue data. The stress gradient in bend specimens reduces the crack driving force into the thickness of the specimen.

## 7.3  Defects and fatigue strength

Fracture surface examination, conventional ultrasonic testing (NDT) and scanning ultrasonic microscopy with different wave types and measuring techniques were utilised to study defects in GRP castings.

Large defects or defect clusters are occasionally present in large castings. They can be detected as part of the normal quality control procedure. Defects larger than $\varnothing 5$ mm would not be permitted in the highly stressed areas of a structure, but by quantifying the negative impact of these defects, decisions can be made if they will be allowed in less highly stressed areas. The long-life constant amplitude fatigue strength of the studied material with unacceptable defects was approximately 50% of the normal material fatigue strength.

Naturally occuring defects are relatively small and are always present in heavy section castings. They cannot be quantified by the standard NDT methods currently used. From a fatigue point of view, shrinkage pores with diameters of several hundred micrometers were found to be most critical. These pores and other associated variations in microstructure affect also propagation of ultrasound which allowed us observing some

correlation between the ultrasonic microscopy (SAM) results and fatigue strength. However, further research would be needed to explain and utilise these results.

Highly stressed areas of castings may contain also defects of intermediate size, which can not be reliably detected or quantified by the standard NDT methods. The studied material contained one such defect in $\varnothing 1$ mm scale (and another outside specimen gauge section). It would have been accepted in real products and the fatigue life of that component would have been less than average. This defect was clearly visible in the SAM images. The lowered fatigue strength and failure initiation site could be predicted before testing this sample.

In principle, these ultrasonic SAM measurements can also be performed in field – even for as cast surfaces using recently at VTT developed contact-free probes. But this technology requires special equipment and expertise and thus is not yet mature for routine engineering use. However, it might be interesting to perform a probabilistic techno-economical study concerning the benefit and cost of finding a defect of, e.g., $\varnothing 1$ mm in size. According to Fig. 20, the probability of finding such a defect in small areas under high stress is rather low, but for high reliability design products having large areas under high stress their importance is raised. Elimination of intermediate size defects from the highly stressed areas would probably improve the reliability of design.

## 7.4  Applications of the weakest link theory

Especially in high cycle fatigue life is dominated by the nucleation and propagation of individual cracks with little observed crack coalescense. The weakest link theory can be helpful in defining strength requirements for high reliability components. For the studied nodular cast iron, the most common weak link can be visualized as the largest near surface shrinkage pore in a region of high stress.

*Notches and size effects*

The greater the surface area of high stress the greater the probability of encountering a pore that will lead to fatigue fracture. This concept allows fatigue data from small test samples to be used in designing very large components and also helps in understanding the effects of stress gradients and notches.

*Distribution of fatigue life*

Careful look at Fig. 16b) would indicate that the scatter in life does not necessarily follow the log-normal distribution for this material. On the contrary, the data looks like there were an upper bound of life. This could be explained, for example, by the

shrinkage pores or graphite nodules as fatigue initiators setting the upper bound together with some distribution of occasional defects reducing the life of individual specimens. However, this is just one observation from one batch of material. A generally accepted opinion is that the log-normal distribution is not always the right one, but determination of the distribution type would become too expensive for practical purposes. Furthermore, for real components, the variation between different melts and other phases of production shall also be accounted for.

*Scatter in fatigue strength and the design curve*

One novel idea developed in this project is to use the concept of weakest link to help develop a better strategy for determining scatter in materials properties. For high reliability designs quantifying the scatter is at least as important as measuring the mean strength. For example, they would both have a similar effect on the design value for failure probability of $1 \cdot 10^{-3}$ only if the error or uncertainty in the standard deviation were one third of the error in the mean endurance limit. This is because the mean value needs to be reduced by 3 standard deviations to obtain a failure probability of $1 \cdot 10^{-3}$.

However, especially in the case of fatigue limit, the standard deviation is much more expensive to measure. After a normal test set of a reasonable size, the uncertainty remaining in the standard deviation is larger than that in the mean value.

The numerical simulations and assessment of different testing strategies showed that when compared to the other methods, the staircase method is powerful (i.e. cost effective) for determining constant amplitude fatigue limits for normal design purposes. However, care should be used in planning the test parameters and in assessment of the significance of the results. A systematic testing strategy for determining both mean strength and design strength should be developed.

*Universal design curve*

Development of the universal fatigue design curve for GRP was partially based on the weakest link theory. This design tool takes the form of the widely used Haigh diagram but takes into account material tensile strength, stress ratio, stress state (torsion or uniaxial) and specimen size effects. A new design tool for nodular cast irons has been proposed and verified for two grades of iron as part of this study. This may be regarded as one of the major technical advances achieved in this project.

# 8. Conclusions

An extensive test program of GRP 500 nodular cast iron has been completed. Fatigue, hardness and tensile tests have been complimented by SEM studies, NDE examination and numerical simulations. Design information for nodular cast iron in the long-life regime has been obtained for both constant and variable amplitude loading. The main conclusions are presented in the following.

### Long-life fatigue

- Based on the data obtained for long finite life tests, empirical rules have been developed to predict the constant amplitude S-N curves for nodular iron in the range of $1 \cdot 10^4$ to $1 \cdot 10^6$ cycles to failure and for mean stresses in the range of 0 to 260 MPa.

### Fatigue under variable amplitude loading

- Lives as long as $1 \cdot 10^8$ cycles to failure were observed using loading histories typical of those observed in rotating or reciprocating machinery.

- This type of data has been published only for a very few number of materials and never before for cast iron. Design models developed for forged materials we investigated but could not applied directly to cast iron. Fatigue modelling remains a difficult problem which should be further investigated.

### Fatigue damage below constant amplitude fatigue limit

- Cycles as small as 60% of the constant amplitude fatigue limit were found to cause significant damage when as few as 1 of 300 000 cycles exceeds the fatigue limit. Miner's sums as low as 0.0001 produced fatigue failures. Similar measurements were made for both smooth and notched specimens.

### Design curve and scatter in fatigue strength

- For high reliability designs, quantifying the scatter is at least as important as measuring the mean strength. But especially in the case of fatigue limit, the standard deviation is much more expensive to measure with a similar reliability.

- The staircase method is cost effective for determining constant amplitude fatigue limits for normal design purposes. However, experience and careful assessment is needed in test planning and in utilising the results. A systematic testing strategy for determining both mean strength and design strength should be developed.

*Universal design curve*

- A new design tool for nodular cast irons has been proposed and verified for two grades of iron as part of this project. Development of the universal fatigue design curve for GRP provides a major technical advance for fatigue design of nodular iron.

- This design tool takes the form of the widely used Haigh diagram but takes into account material tensile strength, stress ratio, stress state (torsion or uniaxial) and specimen size effects.

*Influence of casting size*

- The specimens taken from the largest ingots were clearly the weakest from a fatigue point of view. Fatigue strength of the material taken from the 50×200×300 ingots was approximately 25% greater than the fatigue strength of the material taken from the 200×200×300 ingots.

*Normal shrinkage pores and fatigue strength*

- From a fatigue point of view, shrinkage pores with diameters of several hundred micrometers were found to be important. They cannot be quantified by the standard NDT methods currently used.

- However, these pores and other associated variations in microstructure affect propagation of ultrasound. Some correlation between the ultrasonic microscopy (SAM) results and fatigue strength was observed. Further research would be needed to explain and utilise these results.

*The Murakami-Endo model for fatigue strength*

- The Murakami-Endo model was applied to quantify the effect of micro-pores with some success. However, a single value to describe the hardness of the iron matrix could not be easily defined for this ferritic-pearlitic iron. A method for defining hardness of dual phase matrixes for the Murakami-Endo model would be valuable.

*Defects sizes near the detection limit*

- Defects of intermediate size, which can not be reliably detected by the standard NDT methods, but still reduce notably the fatigue strength, may be clearly visible in the SAM images. This was the case with a defect of $\varnothing 1$ mm size range found

in the studied test material. Elimination of such intermediate size defects from the highly stressed areas would improve the reliability of design.

### *Large defects*

- One set of test material contained defects larger than the acceptability criteria ($\varnothing$5 mm). The negative impact of these defects was quantified. The long-life constant amplitude fatigue strength of the studied material with unacceptable defects was approximately 50% of the normal material fatigue strength.

### *The weakest link theory*

- High cycle fatigue life is dominated by the nucleation and propagation of individual cracks with little observed crack coalescense. The weakest link theory can thus be utilised in defining strength requirements for a component.

- For nodular cast irons the weak link is normally the largest near surface shrinkage pore in a region of high stress. The greater the surface area of high stress the greater the probability of encountering a pore or defect that will lead to fatigue fracture.

### *Notches and Size Effects*

- The weakest link theory and a statistical size effect explains at least part of the effects of component size, stress gradients and notches. This concept can be used to transfer test data to practice. It allows fatigue data from small test samples to be rationally used in designing very large components.

- The scatter in the data, primarily due to the different ingot sizes, seemed to dominate and hide the small differences in fatigue strength expected due to specimen size.

- However, the general relationship between specimen size and scatter has been studied and the results are very promising. Future plans include verifying this concept for other widely used materials.

### *Execution of project*

- The project was successful in obtaining significant results that have already been partially adopted in the participating industry for fatigue design of GRP components.

- The project management was effective. All goals set for the project were met and some new targets were even added along the execution.


## *Recommendations for future work*

As always, many new questions arose, when solving the old ones. In the following we list some open issues which would be well justified research topics either for direct industrial interests or from a general fatigue scientific point of view.

- The universal design curve should be further verified for other GRP grades. The work should target for adopting this new approach for fatigue assessment for wide use in the Finnish industry.

- A systematic testing strategy for determining both mean strength and design strength of endurance limit should be developed for reliable and effective production of design data.

- Static tensile test series for the other ingot sizes should be performed to allow comparison of the size effects in monotonic and cyclic properties. This would be a very small task to support the current results.

- It might be interesting to perform a probabilistic techno-economical pre-study concerning the benefit and cost of finding smaller defects of, e.g., $\varnothing 1$ mm in size in highly stressed areas of the components. The results would be used for estimating whether the topic would be worth of research investment.

- Further research would also be of interest to explain and utilise these results concerning the observed correlation between the ultrasonic microscopy (SAM) results and fatigue strength. This research might be useful for machine design in long term, and in a bit shorter term for cast material quality assurance and development.

- A method for defining hardness of dual phase matrixes for the Murakami-Endo model would be valuable for widening the applicability area of this powerful model.

# 9. Summary

The SCILLED - Spheroidal Cast Iron in Long-Life Design project was realised during the period 1.9.1997 - 31.12.1999. The goal was to gain understanding of the fatigue mechanisms and obtain high cycle design information on GRP500 nodular cast iron under both constant amplitude and variable amplitude loading. All the targets set at the beginning of the project have been achieved with the resources allocated. Several small but technically significant tasks have been added along the course of the project.

The test matrix which was discussed at the first project meeting and agreed on during the second meeting has been performed in full. Part of the test sets were expanded and some were added in agreement between the steering group and the project manager. Table 27 reports how the aimed test matrix given in section 3 of this report has been realised.

In total 332 fatigue tests, 10 tension tests and extensive NDE studies on 36 specimens of GRP 500 iron have been performed. The total number of fatigue cycles applied exceeded $3 \cdot 10^9$ cycles of which the majority were of variable amplitude such as may occur in rotating or reciprocating machines.

*Table 27. Summary of the realised tests and comparison originally aimed test matrix. AP = "as planned"; MTP = "more than planned"; ETP = "extension to plans".*

| Type and purpose of test | Amount of specimens | Comparison to plans |
|---|---|---|
| Tension tests | 10 | AP |
| Smooth specimen endurance limit tests, mean stress 260 MPa | 17 | MTP |
| Notched specimen endurance limit tests, mean stress 260 MPa | 15 | AP |
| Notched specimen long life tests, mean stress –200 MPa | 15 | AP |
| Bending specimen long life tests with R = 0.05 | 20 | AP |
| Bending specimens for size effects | 20 | AP |
| Smooth specimen long life tests, mean stress 182.5 MPa | 15 | AP |
| Smooth specimen long life tests, mean stress 260 MPa | 31 | MTP |
| Notched specimen long life tests, mean stress 260 MPa | 30 | AP |
| Notched specimen tests, mean stress 170 MPa | 15 | AP |
| Smooth specimen variable amplitude loading | 41 | MTP |
| Notched specimen variable amplitude loading | 30 | AP |
| Smooth specimen long life tests, mean stress 0 MPa | 21 | ETP |
| Smooth specimen long life tests with R = 0 | 8 | ETP |
| Notched specimen long life tests, mean stress 200 MPa | 3 | ETP |
| Shear stress long life tests with R = 0 and R – 1 | 13 | ETP |
| Bending specimens with large defects | 15 | ETP |

As the knowledge on fatigue design of nodular iron has been increased, new ideas, questions and recommendations for further work have been generated. These have been partially included in a new project proposal FADEL, which is currently being negotiated for realisation.

# Acknowledgements

# References

Beretta, S., Blarasin, A., Endo, M., Giunti, T. & Murakami, Y. 1997. Defect tolerant design of automotive components. Int. J. Fatigue, Vol. 19, No. 4, p. 319 - 333.

Marquis, G. 1995. High cycle spectrum fatigue of welded components. Espoo: Technical Research Centre of Finland, VTT Publications 240. 83 p. + app. 100 p.

Marquis, G., Rabb, R. & Siivonen, L. 1999. Endurance Limit Design of Spheroidal Graphite Cast Iron Components Based on Natural Defects. In: Fatigue Crack Growth Thresholds, Endurance Limits, and Design, ASTM STP 1372, Newman, J. C. & Piascik, R. S., Eds. West Conshohocken, PA: American Society for Testing and Materials. 14 p.

Marquis, G. & Socie, D. 1999. Long Life Torsion Fatigue with Normal Mean Stresses. Fatigue and Fracture of Engineering Materials and Structures. (Accepted for publication.)

Murakami, Y. 1996. Effects of small defects and inhomogeneities on fatigue strength: Experiments, model and applications to industry. In: Mechanisms and mechanics of damage and failure – ECF 11, Petit, J., de Fouquet, J., Henaff, G., Villechaise, P. & Dragon, A., Eds. Poitiers-Futuroscope, France, 3 - 6.9.1996. Pp. 31 - 42.

Rabb, B. R. 1999a. Determination of the Scatter in the Fatigue Limit. Prepared for TKK Graduate seminar KON-67.204 Statistical Aspects of Fatigue and Fracture, Wärtsilä NSD, Vaasa. 13 p.

Rabb, B. R. 1999b. Fatigue Testing and its Statistical Evaluation into Design Rules. Tampere, Tampere University of Technology Publications 253. 144 p.

Rabb, R. 1999c. Nodular cast iron grade 500-7/ISO 1083 under variable amplitude loading. Wärtsilä NSD Corp., R&C/A2/STRA FA, 21.01.99. 16 p. (Preliminary report.)

Rabb, R. 1999d. Simulation of staircase tests. Wärtsilä NSD Corp., R&C/A2/STRA FA, 16.02.99. 40 p.

Socie, D.F. & Marquis, G.B. 1999. Multiaxial Fatigue. Warrendale, PA: Society of Automotive Engineers. 502 p.

Taivalaho, L. 1999. Effect of casting defects on the fatigue strength of nodular cast iron. Espoo, Helsinki University of Technology. MSc thesis. 84 p.

Wallin, K. 1999. The probability of success using deterministic reliability. In: Fatigue Design and Reliability: ESIS Publication 23, Marquis, G. & Solin, J., Eds. Amsterdam: Elsevier Science. Pp. 39 - 50.

# Appendix A: NDT inspection report of casting with defects

## VALMET
ⴳutpohja Foundry

ULTRASONIC TEST
REPORT NO

| | | | |
|---|---|---|---|
| Inspector | Leo Mäkinen | Date of the test | 8.11.1999 |
| Customer | VTT | Designation/Type | Koepalat |
| Order No | | Drawing No | |
| Pattern No | | Test No | 32,33,34,25 |
| Material | GRP 500 | Surface condition | cast |

Heat treatment
☐ Perlitising
☐ Ferritising
☐ Stress relieving

| | | | |
|---|---|---|---|
| Procedure | | Apparatus | Krautkrämer USN 50 |
| Calibration | AVG Ø3,5,8 mm | Couplant | Liisteri |
| Probe | SEB2E0° | Gain setting | 60,53,46Db |
| Transfer correction | | Additional gain setting | |

Location of the examination

Supplementary data
    Katso liitteet. 5kpl.

Test result
☐ Meets the requirements
☐ Does not meet the requirements

8.11.1999

Accepted by
Leo Mäkinen

| | | Varebetegnelse / Item desciption: | | | | | | | | Varenr. / Item No: |
|---|---|---|---|---|---|---|---|---|---|---|

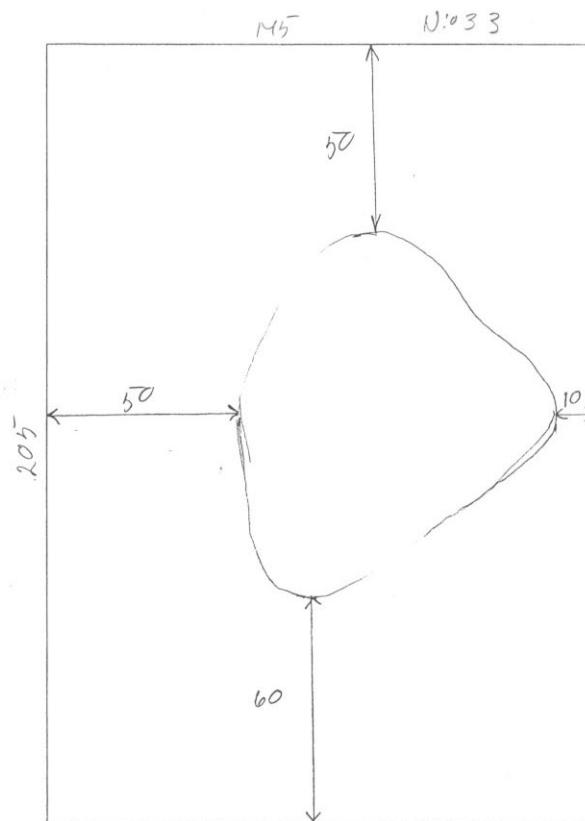| Charge No: | | Kontrolleret af - Dato / Inspected by - Date: | | | | | | | Leverandør / Supplier: |
|---|---|---|---|---|---|---|---|---|---|
| | | 8.11.1777  L. Mäkinen | | | | | | | |

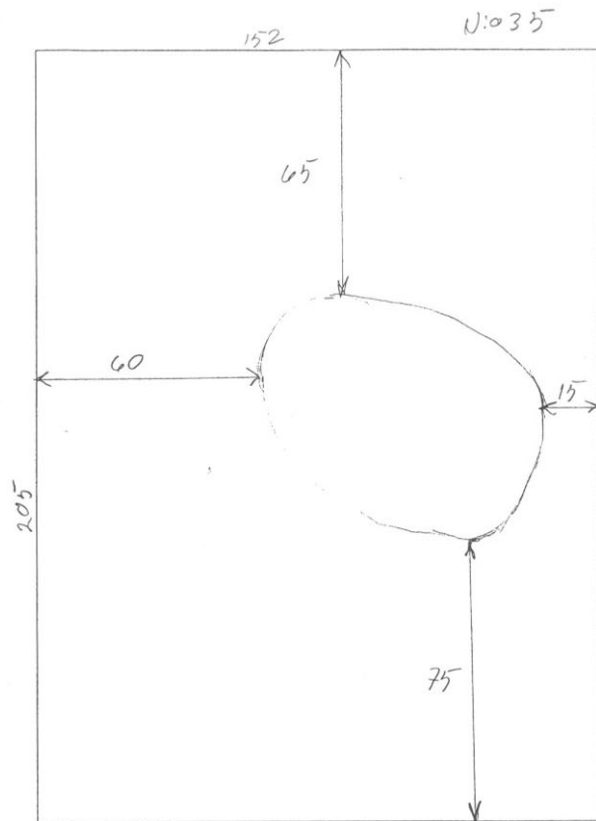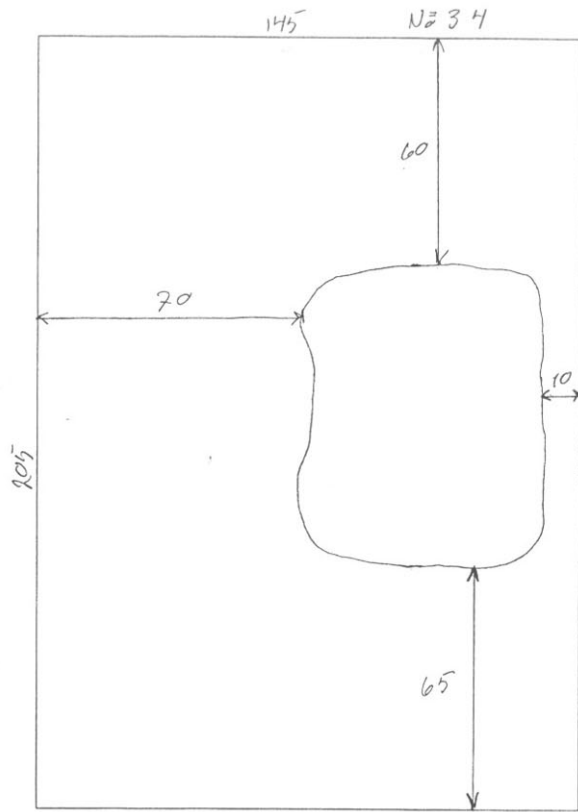| No/ Nr | projected area/ projiceret areal (mm x mm) | Location/ Placering | | cross section/ tværsnit (mm) | Depth extension / KSR Dybdeudbredelse / KSR | | loss/ tab (dB) | Evaluation/ Bedømmelse | | remarks/ bemærkninger |
|---|---|---|---|---|---|---|---|---|---|---|
| | | area/ areal | zone/ zone | | ext. / KSR/ udv. / KSR (mm / KSR) | int. / KSR/ indv. / KSR (mm / KSR) | | appr/ godk. | fail/ kass. | |
| 32 | 80×120 | | | 52 | 24/73 ∠8 | 21/73 ∠8 | | | | |
| 2 | | | | | | | | | | |
| 33 | 90×90 | | | 52 | 20/73 ∠8 | 23/73 ∠8 | | | | |
| 4 | | | | | | | | | | |
| 34 | 70×70 | | | 52 | 23/73 ∠8 | 20/73 ∠8 | | | | |
| 6 | | | | | | | | | | |
| 35 | 60×90 | | | 52 | 22/73 ∠8 | 23/73 ∠8 | | | | |
| 8 | | | | | *) | | | | | |
| 9 | | | | | | | | | | |
| 10 | | | | | | | | | | |
| 11 | | | | | | | | | | |
| 12 | | | | | | | | | | |
| 13 | | | | | | | | | | |
| 14 | | | | | | | | | | |
| 15 | | | | | | | | | | |

Remarks/bemærkninger: Kaikissa virheissä an yksittäisiä
⌀5 mm:n käyrän ylityksiä.

*) Tällepudelle on piirretty vika alueen ääri viivat

165

40

75

195

15

25

№ 32

145

N:033

50

205

50

10

60

A3

№ 34

145

70

60

205

10

65



U:035

152

65

60

205

15

75

A4

Author(s)
Marquis, Gary & Solin, Jussi

Title

# Long-life fatigue design of GRP 500 nodular cast iron components

Abstract

A project on Spheroidal Cast Iron in Long-Life Design was realised in 1997 to 1999. The goal was to gain understanding of the fatigue mechanisms and obtain high cycle design information on GRP500 nodular cast iron under both constant amplitude and variable amplitude loading. All the targets set at the beginning of the project have been achieved with the resources allocated. Several small but technically significant tasks have been added along the course of the project.

In total 332 fatigue tests, tension tests and extensive NDE studies on GRP 500 iron have been performed. The total number of fatigue cycles applied exceeded $3 \cdot 10^9$ cycles of which the majority were of variable amplitude such as may occur in rotating or reciprocating machines.

Empirical rules have been developed to predict the constant amplitude S-N curves for nodular iron in the range of $1 \cdot 10^4$ to $1 \cdot 10^6$ cycles to failure and for mean stresses in the range of 0 to 260 MPa. A new design tool for nodular cast irons has been proposed and verified for the two iron grades studied in this project. This design tool takes the form of the widely used Haigh diagram but takes into account material tensile strength, stress ratio, stress state (torsion or uniaxial) and specimen size effects.

Cycles as small as 60% of the constant amplitude fatigue limit were found to cause significant damage when as few as 1 of 300 000 cycles exceeds the fatigue limit. Miner's sums as low as 0.0001 produced fatigue failures. Similar measurements were made for both smooth and notched specimens.